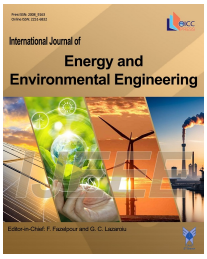

Int. J. Energy Environ. Eng 2024; 15(1) : 1-26

International Journal
of
Energy and Environmental Engineering (IJEEE)

https://doi.org/10.57647/ijeee.2024.1501.08

Assessment of Techno-Economic Hydro and Solar Power Energy Potential in Rural Region of Kulfo Catchment, Rift Valley Ethiopia

Mesay Feleke Negash, Getachew Bereta Geremew*, Melkamu Teshome Ayana, Otoma Orkaido Garo

Faculty of Hydraulic and Water Resources Engineering, Arba Minch Water Technology Institute, Arba Minch University, P.O. Box 21, Arba Minch, Ethiopia

***Corresponding author:** getachewbereta@gmail.com

Original Research

Abstract:

Eighty-five percent of Ethiopia's population lives in rural areas, where only 36% have access to electricity. This study aimed to assess the techno-economic potential of hydro and solar power for rural regions in the Kulfo catchment using the Hybrid Optimization Model for Multiple Energy Resources (HOMER). Data from hydrologic, meteorological, and ERA5 reanalysis sources, along with household surveys, were used to analyze electricity demand. The selected sites, including T'sayte, Wisamo, Mayzo Doysa, and Gatse, were evaluated for run-of-the-river micro-hydropower and solar hybrid system potential was selected for this study. The HBV-IHMS model estimated stream flow at the sites, with Nash-Sutcliffe efficiency (NSE) of 0.69 for calibration and 0.63 for validation. Energy use in the selected areas was 19.77%, while 80.2% of energy went unused. The annual power production from solar photovoltaic (PV), hydropower, and generators was 5,641,903 kWh, 27,566,199 kWh, and 11,736,523 kWh, covering 12.6%, 61.3%, and 26.1% of the energy needs, respectively. The levelized cost of energy (LCOE) was 0.0962 dollars per kWh, slightly higher than the Ethiopian Electricity Corporation's cost of 0.06 dollars per kWh.

Keywords: Kulfo Catchment; Techno-Economic Hydro and Solar Power: HOMER; HBV-IHMS model; Levelized cost of energy; Renewable energy

Cite this article: Negash M. F., Geremew G. B., Ayana M. T., Orkaido Garo O., Assessment of Techno-Economic Hydro and Solar Power Energy Potential in Rural Region of Kulfo Catchment, Rift Valley Ethiopia. Int. J. Energy Environ. Eng. 2024; *15*(1) : 1-26 https://doi.org/10.57647/ijeee.2024.1501.08

1. Introduction

The world's energy consumption is estimated at 22 billion Wh per year [1]. Energy has been considered a critical source for socio-economic development and is critical to solving the challenges faced by sub-Saharan African countries in providing energy services [2, 3, 4]. The rate of access to advanced electricity in African countries such as Egypt, Algeria, Tunisia, and Morocco has indeed reached 100 %. Even though countries in the central region such as South Sudan (15%), Chad (13.8%), the Central African Republic (14%), and the Democratic Republic of the Congo (19%) are highly inaccessible (below 20%) [5]. Except in the middle section of the African continent, the urban areas have been average level of electricity coverage higher than the rural areas. In Ethiopia, urban areas have access to electricity more than 90% of the population [6]. However, the rural region, comprising 85% of the population, has electricity coverage that is only 36% of the nominal average, and 58 million people have no access to electricity [7, 8].

In most developed countries the spread of hydro-

meteorological stations is much denser compared to developing and poor countries [9, 10].A sizable portion of Ethiopia's population lacks access to electricity [11, 12]. Presently, the reliability and sustainability of many standalone hybrid systems are highly vital issues. Accordingly, in terms of producing power without degradation integrating hybrid systems hydro and solar PV arrays provides several advantages over standalone systems [13, 14]. The current study aims to assess the techno-economic of hydro and solar energy to electrify the rural village of Kulfo Catchment, integrating ERA5 satellite information and HOMER [15]. HOMER is a hybrid optimization model for renewable energy applicable to assessing the technical and economic viability of standalone and hybrid energy systems in single to multiple with highly detailed information [16, 17, 18]. ERA5 is the most recent climate re-analysis freely available online with full climate variables for the current and future potential energy assessments [19, 20, 21, 22]. Ethiopia possesses immense renewable energy potential, with its hydroelectric resources estimated at 45,000 MW and solar irradiation averaging 4.5-7.5 kWh/m^2/day, translating to a technical solar potential of ~1.3 million GWh/year. Despite this, the country's currently installed capacity is a fraction of this potential, with hydro at approximately 4,500 MW (primarily from the Grand Ethiopian Renaissance Dam) and grid-connected solar at just 750 MW, leaving over 90% of the hydro and ~99.9% of the solar potential untapped [23].

Energy has been the foundation of every action and instant of human life in all industries [24]. Hence, modern time energy has been chosen for measuring a nation's economic development [25, 26, 27]. The contribution of clean, inexhaustible, and sustainable energy sources to minimizing the current environmental pollution the world has been facing is immense [28]. Different countries have implemented various modern technologies to enable the green energy idea for the benefit of society, such as small and mini hydropower [29, 30].

Most greenhouse gas emissions can be reduced by using renewable energy, which can also supply two-thirds of the world's energy needs [31, 32] Hydro and solar photovoltaic (PV) technologies have a high level of energy efficiency. The need to find renewable alternatives and non-polluting energy sources takes precedence [33]. The significance of hydro and solar energy sources in raising and improving the living standards of people in rural areas provides different services to numerous commercial centers, healthcare facilities, and irrigation systems [23, 34]. The risk of respiratory and lung disease has been the most serious effect of burning biomass in the household [35]. According to the World Health Organization, each year 1.6 million people die prematurely; more than half of these people die because of indoor smoke inhalation, and children under the age of five are the ones who die. According to the International Energy Agency (IEA), the number of people who cook with biomass may increase to over 2.7 billion by 2050 [36]. According to a recent study, 900 million people throughout the world lack access to dependable and affordable energy, which is the primary cause of rising poverty and the decline of society's socioeconomic [37]. The annual power production of solar energy (PV), hydropower, and generators was 5,641,903, 27,566,199 and 11, 736, 523, kwhr/yr and the percent coverage of 12.6%, 61.35, and 26.1% respectively. Remote rural areas face significant challenges in electrification due to their distance from the national grid, rugged topography, and low population density, which make grid extension economically unfeasible. For instance, in the Kulfo Catchment, where over 80% of the population lacks access to electricity, grid expansion would require substantial investment in infrastructure that cannot be justified by the low energy consumption of scattered households. These economic constraints are further compounded by the region's poor road access and the high cost of materials, which hinder the delivery and maintenance of grid components. As a result, decentralized solutions like micro-hydro and solar hybrid systems offer a more viable alternative for such off-grid communities.

2. Method and Material

2.1 Description of the study area

The Kulfo watershed is found in the Rift Valley and is geographically located at 5°48´ to 6°12´ N and 37°21´ to 37°35´ E, with a total area coverage of about 380.4 square kilometers. The elevation of the catchment ranges from 1230 to 3570 m (a.m. s.l.).The current study site lies at the middle to lower reach of the Kulfo River, near the town of Arba Minch, extending between 6°1´50´´ and 6°2´45 N and 37°32´38´´ and 37°34´35´´ E. In addition, settlements and agriculture occupy around 28.9% of the catchment usage. The river forms at the junction of the Titika and Gulando rivers. The outflow of Abaya was joined by the inflow to Lake Chamo at 5°55´ N latitude and 37°33´ E longitude and at 6°7´ N latitude and 37°27´ E longitude. The region experiences a bimodal distribution of rainfall, with the lower catchment receiving 959 mm and the upstream watershed receiving 1390 mm. The yearly average temperature in the upstream area is 16.7 °C, and the downstream area temperature is 24°C [38]. The detailed study area is described below in Figure 1.

Topography and Slope

The shape and relief of the land surface are determined by the slope and topography. Topography is a measurement of elevation, and the slope is the percentage change in that height (topography) over a specific distance. To measure topography, lines are drawn between locations of equal height (contour). While slope was calculated by dividing the elevation difference between two places by the lateral distance between them, the topography of the watershed varies significantly. The watershed outlet has a maximum elevation of 3570 and a lowest elevation of 1230, as indicated in the Figure 2. These topographical variances play a vital role in the variation in rainfall

https://doi.org/10.57647/ijeee.2024.1501.08

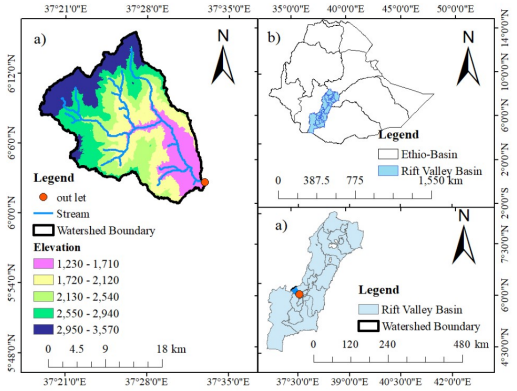

Figure 1. Location of study area

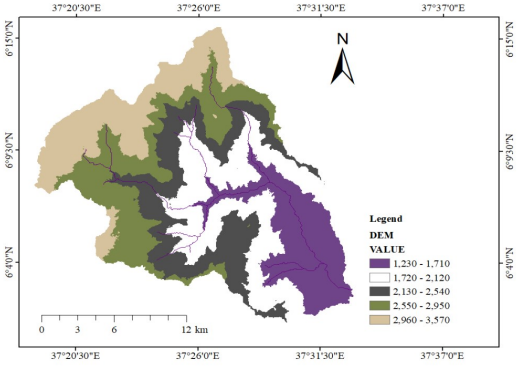

Figure 2. Classification of elevation of the watershed

patterns and other meteorological factors.

2.2 Data collection method

The detailed information on the collected data and models used in this research in Table 1

2.3 Methodology

Selection of the Beneficiary Community

The stratified random sampling method was the one chosen by the Kebeles. The process of separating population members into uniform subgroups prior to sampling is known as stratification (Male and female). In this instance, we begin by splitting the population into various strata based on their attributes, such as male, female, rural, and urban, and then randomly selecting a sample from each stratum. Next, we select a random sample from each stratum in each of those sections; the final sample is the sum of the samples from all the strata. To understand more about the beneficiary community. They acquired some information from historical rivers when measuring the observed heads. Four rural selected kebeles lacked electricity based on a brief conversation done during the head measurement. It is useful to know the names and locations of the communities, as shown below in Table 2.

Quality assessment of hydro-metrological data

Accessibility data about the hydrological, metrological, spatial, and satellite data in the studied area were collected from different sources. The class of the metrological station ranges from class 1 (synoptic stations), which records almost all the climate parameters, to class 4, which records only precipitation. The study area was five meteorological and one stream flow gauging station data have been used. On Arba Minch station the metrological data ranges from 1991–2017 and the stream flow data covers a period from 1991 to 2013. However, both sets of data have numerous gaps and absent values varying between a day and a year. The absence of organized stream flow data significantly hampers accurate assessment of hydropower energy potential, as it prevents reliable estimation of flow variability, seasonal patterns, and long-term availability of water resources. This limitation often forces researchers and developers to rely on assumptions or extrapolated data, increasing the risk of over- or underestimating project feasibility and sustainability [39]. The available meteorological and hydrological data for their location are described as shown below in Table 3.

The above Table 3 shows that the available metrological data of the selected five stations, namely Arba Minch, Chencha, Daramalo, Gerese, and Kamba were obtained from 1991-2017.

Table 1. Description of data and models used in this study

Data Type	NO. Data	Source	Use
Primary Data	Site selection Head drop	Field survey	For placement of electromechanical equipment
	Cost of Energy	EPCO	Input for HOMER model
Secondary Data	Hydrological and Metrological Data	From NMAE and MoWE	Input into HBV-IHMS & HOMER Obtained input data
	(ERA5) Satellite	https://ecmwf.int/en/fore/casts /datasets/reanalysis-datasets/era5/	To determine catchment parameters
	DEM (30X30) LULC	https://gdem.cr.usgs.gov/ https://earthexplorer.usgs.gov	LULC classification
Software	HBV-IHMS	SMH	To simulate stream flow To process the NetCDF file
	GrADs	http://sourceforge.net/projects /opengrads	To calculate the optimal configuration of the hybrid energy system, LCOE and NPC
	HOMER 4.11	www.homerenergy.com	

Table 2. The chosen kebeles coordinates were measured

No	Zone	Woreda	Kebele	x	y	z
1	Gamo	Gacho baba	Wisamo	6.12	37.42	2020
2	Gamo	Gacho baba	Mazodoysa	6.18	37.43	2392
3	Gamo	Gacho baba	Gatse	6.12	37.45	1703
4	Gamo	Gacho baba	T'sayte	6.15	37.47	1717

Table 3. Availability of metrological Data with their Location

Station name	Latitude (°)	Longitude (°)	Elevation (m)	metrological Data Availability
Arba Minch	6.06	7.56	1220	1991-2017
Chencha	6.23	7.58	2632	1991-2017
Daramalo	6.30	7.40	1183	1991-2017
Gerese	5.92	7.30	2329	1991-2017
Kamba	6.05	7.20	1895	1991-2017

Table 4. Stream Flow data contemplate in this study

Station Name	Latitude (°)	Longitude (°)	Elevation (m)	Availability	Catchment Area (km^2)
Arba Minch	6.06	7.56	1220	1991-2013	380.4

https://doi.org/10.57647/ijeee.2024.1501.08

The research area has been one gauge station gained from Arba Minch station with available data from 1991–2013. In addition, the catchment area was 380.4 km^2 as shown in Table 4 above.

2.4 Filling Missing Rainfall Data

Data on measured rainfall is critical to solving various issues in hydrological research and design. In the case of periodic observation gauges, missing data may occur if the observer does not make the required trip to the gauge. Another issue that leads to insufficient data records is the loss of recording gauges, and devices that fail due to mechanical or electrical failure may also not record all the data that should be recorded. Data processing and analysis must therefore be carefully considered because they may yield ambiguous and inconsistent conclusions that are at odds with the situation as it actually stands. Several approaches have been proposed to predict the missing rainfall. The arithmetic mean, inverse weight distance, graphical correlation, normal ratio, and linear regression methods are among them [40, 41]. The Inverse Distance weights method is as given in Equation 1.

Inverse Distance Weights Method

The weights assigned to each sample in this method are inversely correlated with how far away the location being estimated [42].

$$P_x = \frac{\sum_{i-1}^{n}\left(\frac{P_i}{d^2}\right)}{\sum_{i-1}^{n}\left(\frac{1}{d^2}\right)} \quad (1)$$

Where d is the distance from each location, the point being estimated, P_X is the station's expected rainfall, P_i is the rainfall values of the rain gauges utilized for estimation, and N is the number of nearby stations. In order to complete the missing meteorological data for this investigation, the inverse distance approach was chosen. This method is better because the distance between stations would be taken into account and most climate data spatially varies with distance.

2.5 Regression methods

Finding the value of a dependent variable (y) for a given value of the independent variable (x) is done using linear regression, a straightforward supervised learning technique. It effectively models a linear relationship between the variables input (x) and output (y). The basic method that can be quickly put into practice and yield fantastic outcomes. In addition, unlike other complicated methods, these models may be trained rapidly and successfully on systems with little processing capability. This approach was used in this thesis to fill in the streamflow data that was missing. The value of a dependent variable (y) for a given value of the independent variable (x) can be predicted using a straightforward supervised learning technique that efficiently models a linear relation between the input (x) and output (y) variables in the form of $Y = mx + c$ using a given dataset [43].

2.6 Quality assessment of ERA5 Satellite data

The assessment of water resource regions and the effective design of water resource initiatives. The evaluation of energy sources and climate forecast studies all greatly benefit from reliable and accurate climate data. Daily climate records are hardly ever inclusive, resulting in frequent and extended intervals of missing readings. The gaps and discontinuities in the historical meteorological data can be filled by gridded satellite climate data [44]. The European Centre for Medium-Range Weather Forecasts (ECMWF) released the updated climate reanalysis dataset ERA5, which was used to determine the climatic parameters of the selected energy locations. The information has been available since 1978 and is updated hourly. However, this analysis examined data from 1991 to 2020 on average hourly rainfall, temperature, wind speed (u and v components), surface solar radiation, and cloud cover. ERA5 was chosen due to its many advantages, including the availability of all the meteorological variables needed for this investigation at a relatively high resolution (31 × 31 km). The information in NetCDF format was obtained from http://ecmwf.int/en/forecasts/datasets/reanalaysis-datasets/era5.

The available historical hydro-meteorological data of the Kulfo catchment ranges from 1991 to 2017, with long years of missing data for some of the stations. Satellite data downloaded from the ERA-5 website was used to obtain well-informed data about the catchment and to fill in the missing data in the catchment. Satellite data encompassing precipitation, dry and wet surface solar radiation, minimum and maximum temperature, wind speed, and dry and wet cloud cover were downloaded from six grid center points (GCPs) in the Kulfo watershed. Every grid point is represented by the notation Kxy, where K stands for the grid point and x and y stand for multiple rows and columns from the catchment's southernmost points to its westernmost point, respectively. The data length covers a period from January 1, 1991, to February 20, 2022. As shown in Figure 3 below, provides the location of the satellite data and the satellite data with the hydro-meteorological stations.

Bias correction of ERA5 Satellite data

The mostly objective representations of observed historical climate data that satellite outputs provide require quick adjustment methods. The main source of the biases is systematic mistakes in the hydrologic model, which may cause the model parameters to be overestimated or underestimated [45, 46, 47]. Consequently, before goods are utilized as input, satellite climate data must be rectified. There are numerous bias correction techniques available to get rid of the mistakes in the satellite output. In this work, biases in temperature and precipitation were corrected using variance scaling (VARI) and power transformation method (PT), respectively [48, 49]. The techniques rely on comparing the satellite outputs' mean and coefficient variation to the climate data that has been observed.

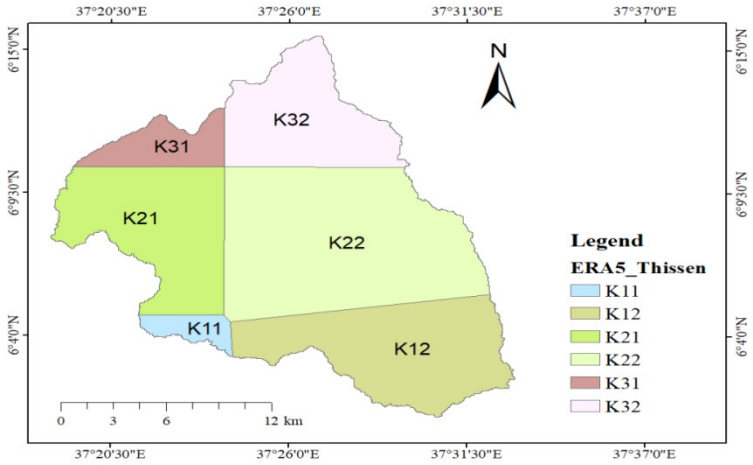

Figure 3. Thiessen polygon of ERA5

Power transformation (PT) of precipitation

The most popular method used to correct bias in satellite products is the power transformation. The technique relies on the idea of reducing the mean and variance errors between satellite and observed rainfall data. The data at the chosen energy site was correct, taking into account the area of rainfall in the satellite data and the observed data. Equation 2 shows the power transformation method used in this study.

$$P_c = aP_0{}^b \tag{2}$$

Where a and b are the bias correction factors for mean and variance respectively, and P_c is the bias corrected ERA5 rainfall and P_0 is the uncorrected ERA5 satellite rainfall.

The bias factor (a) value was established, the transformed ERA5 mean was equal to the gauge observations mean, and bias factor b was iteratively found so that the satellite's coefficient of variance (b) matched the observed daily rainfall data. Generally, the noticed and satellite-biased corrected precipitation is shown below in Figure 4.

Figure 4 above compares rainfall data from satellites and observations. Observed an average monthly rainfall peak of 6mm during April. However, it dropped in December and after bias correction, rainfall reached a peak of 4mm in October.

Variance scaling (VARI) of temperature

It was commonly known that both observed and satellite temperature data are normally distributed, the PT approach is unable to correct temperature biases in satellite data. The VARI process modifies the temperature settings until the observed mean and variance are consistent with the satellite data. The governing VARI equation was described in Equation 3

$$T_{cor,m,d} = [T_{raw,m,d} - \mu(T_{aw,m}] \times \frac{\sigma(T_{obs,m})}{\sigma(T_{raw,m})} + \mu(T_{obs,m}) \tag{3}$$

Where, $T_{cor,m,d}$ is corrected temperature on d^{th} day of the m^{th} month, and $T_{raw,m,d}$ is the raw temperature on the d^{th} day of the m^{th} month. $\sigma(T_{obs,m})$ and $\sigma(T_{raw,m})$ represents the standard deviation of observed and raw temperature at a given month respectively. $\mu\left(T_{raw,m}\right)$ and $\mu\left(T_{obs,m}\right)$ represents the mean value of observed and raw temperature at a given month respectively. The observed and satellite biased corrected temperature as shown below in Figure 5.

2.7 Determination of areal rainfall

Rainfall is never been evenly distributed in the catchment or basin while it varies geographically in terms of duration and intensity. This study used the weighted mean method. The method is better suited to modestly sized areas with fewer rainfall stations than the basin's area and some challenging terrain. The average yearly precipitation across the entire basin was determined in this thesis using data from rain gauges using the Thiessen polygon method in equation 4.

$$P_{average} = \frac{\sum_{i=1}^{n}(P_i \times A_i)}{A_i} \tag{4}$$

Where, n is the number of stations of P_1, P_2 & P_3. A_1, A_2, and A_{n-1} denote the area of each station. P_i is the representative precipitation, and A_i is the area of the surrounding.

The amount of rain at a specific location is represented by a rain gauge station. Rainfall changed at this point of aerial precipitation. One of the most crucial criteria in hydrology is the depth of rainfall when considering an enclosed area. The Thiessen polygon method is used to calculate the average annual rainfall. Areas represent rainfall that varies in intensity and duration horizontally from place to place. Each metrological rainfall station data should be weighted by the Thiessen polygons created with Arc GIS 10.3 software. Each gauge area of effect is described in Table 5 and Figure 6 below.

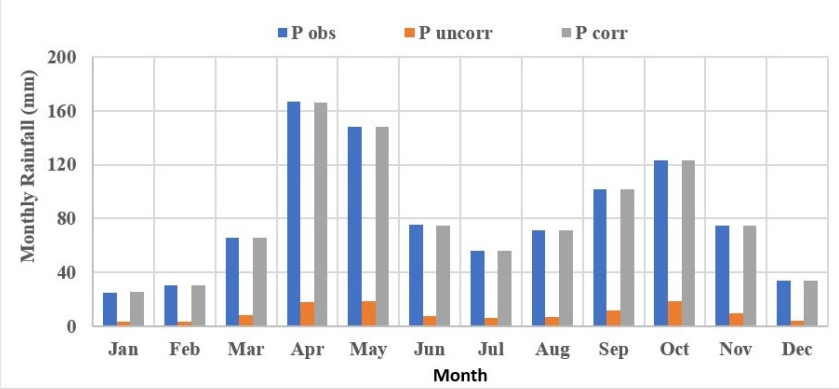

Figure 4. Comparison of observed against bias corrected precipitations

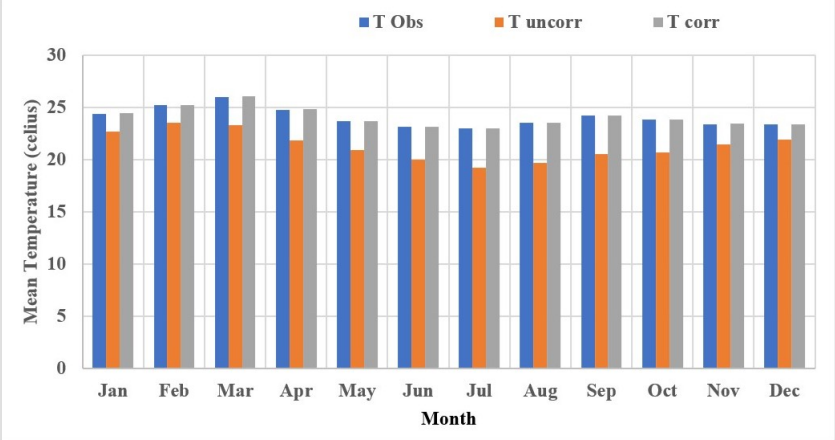

Figure 5. Comparison of observed against bias-corrected satellite mean temperature

Table 5. Thiessen polygon National Metrology Agency of Ethiopia (NMAE) Station

ID	Name	Area	Thiessen Weight (%)	Perimeter
1	Arba Minch	204.082	53.6433	477.939
2	Chencha	21.9371	5.7662	433.686
3	Dara Malo	145.737	38.3072	468.91
4	Gerese	7.06654	1.8575	369.545
5	Kemba	1.61996	0.4258	318.756
	Total	380.4	100	2068.836

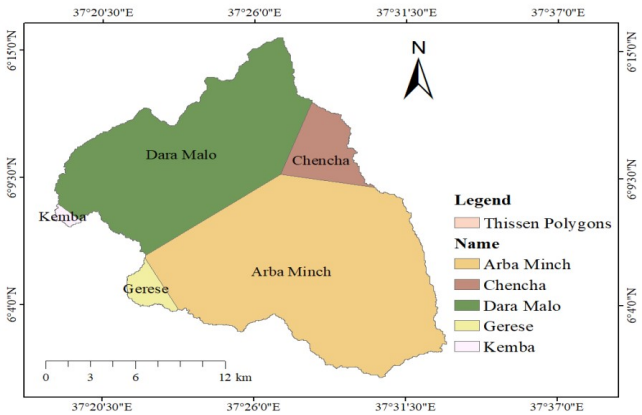

Figure 6. Thiessen polygon National Metrology Agency of Ethiopia (NMAE) Station

https://doi.org/10.57647/ijeee.2024.1501.08

2.8 Data Quality Consistency Test

Data consistency is determined by testing and adjusting available rainfall data, especially when weather circumstances that are pertinent to the rain gauge station have changed significantly, resulting in data inconsistency. To determine the consistency of the rainfall record, the double mass curve (DMC) method compares the gathered monthly or annual rainfall of the station which is expected to be inconsistent with the concurrent accumulated mean annual rainfall of a group of nearby rain gauge stations known as the base station. The station's recorded data must be efficient by the calculation utilizing equation 5 if there is a change in the slope of the curve.

$$P_{cx} = P_x \times \frac{M_c}{M_a} \tag{5}$$

Where P_{cx} represents corrected precipitation at any period, P_X represents the originally recorded precipitation at that period, M_c represents the corrected slope of the double mass curve and M_a represents the original slope of the double mass curve.

The quality and dependability of data gathered from weather stations are influenced by numerous factors. Their location, the tool, the technique employed and the caliber of the observations influence precipitation stations, so the time series may become inhomogeneous. Therefore, statistical testing should be done to determine the reliability and quality of the data that will be utilized in the modeling of hydrology and water resource processes. When choosing a representative meteorological station to analyze areal rainfall, it is essential to verify the homogeneity of group stations. The non-dimensional values of each station's monthly precipitation were calculated using the following equation 6.

$$P_i = \left(\frac{P_{i,av}}{P_{av}}\right) \times 100 \tag{6}$$

Where P_i is the non-dimensional value of precipitation for the month in stations i, $P_{i,av}$ is over the year average monthly precipitation for station i, and P_{av} is over the year's average yearly precipitation of station i.

Outliers are observations or measurements that are uncertain because they are substantially smaller or much greater than the vast majority of the observations. These observations are troubling because they may not be generated by the mental process under consideration or may not represent the ability under consideration. The issue is that a few outliers can occasionally affect group results by altering the mean performance, increasing variability [50].

2.9 HBV model into Kulfo Catchment

For continuous calculation runoff, the HBV model is best characterized as a semi-distributed conceptual model that incorporates conceptual numerical descriptions of hydrological processes. The HBV was originally developed by SMHI in the early 1970s to assist hydropower operations and it was named after the abbreviation Hydrological Byrains Vattenbalans-avdelning (hydrological bureau water balance section). Daily discharge is simulated by the HBV model utilizing calibration data from temperature, rainfall, potential evapotranspiration, and daily runoff. The model routine includes a transformation function, a basic routing process, and a response routine for precipitation and snow buildup. For soil moisture accounting, as seen in Figure 7, groundwater recharge and real evaporation are combined.

Model structure

The model uses temperature, potential evaporation, and daily precipitation as inputs to simulate daily discharge. Whether the temperature is above or below a threshold temperature determines whether precipitation is simulated as rain or snow. Furthermore, stream flow information is necessary for calibration. Sub-Rivers are the main hydrological units used in the model. Rivers with significant elevation range can be subdivided into elevation zones, and a straightforward land use classification can be created [51]. As indicated in Figure 8 HBV model structure representation.

Precipitation and snow accumulation routine

Input data for the HBV model include daily precipitation, daily temperature, and long-term monthly or daily evaporation temperature. In the subroutine for precipitation and rainfall, a threshold temperature is used. However, in this study, the subroutine for precipitation and snow accumulation was applied in the form of only rainfall Equation 7.

$$RF = P_{corr} \times rfcf \times P\,, \quad \text{If } T > tt \tag{7}$$

Where: RF is the rainfall, P is the observed precipitation (mm), Tis the observed temperature (°C), Tt is the threshold temperature (°C), rfcf is the rainfall correction factor, and P_{corr} is the general precipitation correction factor

2.10 Model Sensitivity Calibration and Validation at Kulfo near Arba Minch

Many of the tributaries lack adequate hydro-meteorological stations, and even the main course was gauged at one location. Consequently, obtaining historical hydro-meteorological data for the chosen energy site becomes a challenge. The only other option is a model to simulate stream flow using HBV-IHMS with complete calibration and validation. The fit between the simulated and observed data determines the acceptability of the model output. The fitness of the simulation result is determined by the model parameters, which must be kept within a reasonable uncertainty range. Before calibrating and validating the IHMS model, a parameter sensitivity analysis was performed to identify the most sensitive parameter representing the catchment. This helps in focusing on the most sensitive parameters during the calibration and validation processes. The sensitive parameters are fuel price, stream flow, PV capital cost, generator capital cost, and storage system capital

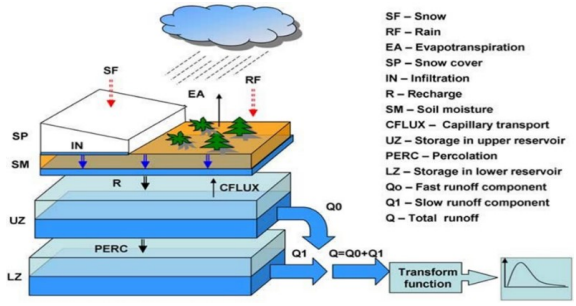

Figure 7. Schematic representation of the HBV model

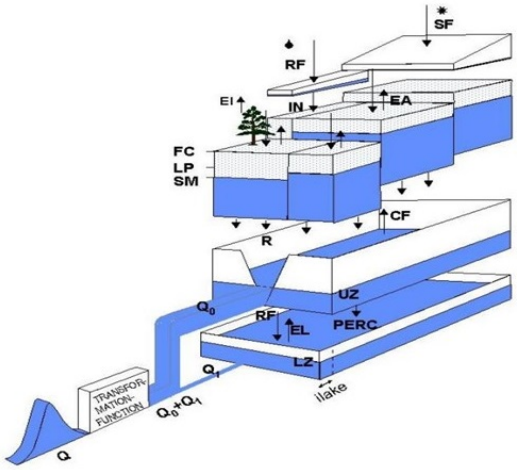

Figure 8. HBV model structure representation

cost used the calibration and validation processes. The process of calibrating a model involves figuring out the parameters that most closely match the simulated and observed runoff from a watershed. This model supports both automatic and manual calibration, which are two of the many methods for determining the optimal parameter configuration. For calibration, thirteen years of measured flow data from the period of January 1, 1993, to December 31, 2006, were employed and January 1, 1991, to December 31, 1992 year used for the warm up period.

After calibrating the model and determining the optimal parameters, it must be verified using arbitrarily observed flow data. The model was validated using an independent measured flow data set spanning seven years, from January 1, 2007, to December 31, 2013.

A sensitivity study of the risks to renewable energy systems in the Kulfo Catchment should assess how weather variability (such as variations in streamflow or solar radiation) and extreme weather events (such as droughts or heavy rainfall) affect energy output and costs. The levelized cost of electricity (LCOE) would rise as a result of increased reliance on backup generators due to decreased hydropower output from low rainfall or decreased solar generation during cloudy times. By measuring these risks, the study can determine ways to mitigate them, like maximizing battery storage or varying energy sources, to improve system resilience and guarantee rural areas have a steady, affordable supply of electricity.

Model Performance Evaluations

The accuracy and reliability of the IHMS models were evaluated using statistical methods and compared to observed values. To assess the accuracy of streamflow calibration and validation, various statistical indicators such as Nash-Sutcliffe modeling efficiency (NSE) and relative volume error.

The Nash Sutcliffe Efficiency (NSE), which ranges from $-\infty$ to 1, is a metric that quantifies how well the observed Vs simulated value plot matches. A value of 0 indicates that the gauge mean is as good as the estimate; a value of 1 indicates that the gauge measurements and the satellite-based estimates match exactly, and a value of negative indicates that the gauge mean is better than the estimate. It is computed by the following equation 8.

$$NSE = 1 - \frac{\sum_{i=1}^{n} (Q_{obs,i} - Q_{sim,i})^2}{\sum_{i=1}^{n} (Q_{obs,i} - Q_{obs,mean})^2} \quad (8)$$

The volumetric inaccuracy of the simulated streamflow was measured using Relative Volumetric inaccuracy (RVE), which has values between $-\infty$ and $-\infty$. While

https://doi.org/10.57647/ijeee.2024.1501.08

RVE between -10% and -5% and 5% and 10% will indicate satisfactory performance, as indicated by equation 9, the model performs best when the RVE is near zero and very well for RVE between -5% and 5%.

$$RVE = \frac{\sum_{i=1}^{n} (Q_{sim,i} - Q_{obs,\,i})}{\sum_{i=1}^{n} (Q_{obs,i})} * 100\% \quad (9)$$

2.11 Selection of potential sites in Kulfo Rural Kebele

The selection was site assessment, civil work, electromechanical work, and energy demand for the environment. The potential sites for hydropower and solar development have been chosen using the multi-criteria analysis (MCA) technique based on the available data. MCA is a method for answering a variety of technical and economic issues that arise during the selection of sites for energy development based on a variety of parameters [52]. In my study, five class criteria have been recommended. This contained technical, economic, environmental, social, and other criteria related to safety and reliability that were considered to assess the most feasible arrangement with its suitable site. The detailed summaries of the groups of criteria used are illustrated in Table 6.

2.12 Energy Assessment Using Hybrid Optimization Model for Electrical Renewable Energy (HOMER)

The hybrid hydro and solar systems' ideal energy production was ascertained using HOMER. This design optimization model selects the load management, dispatch, and configuration strategies. There are two different types of HOMER software available: HOMER Pro and HOMER Grid, for all forms of distributed generation systems, distant utilities, and micro grids. Grid-connected solar plus storage or other grid-connected hybrid distributed generation systems were techno-economically optimized using HOMER Pro. Both programs have a 21-day expiration date and are available upon request from the HOMER Energy website. This study used HOMER Pro version 4.11 to maximize the techno-economic viability of solar and hydro systems in Kulfo catchments. Before running the HOMER simulation, the study selected specific components to model the hybrid energy system: solar panels (photovoltaic arrays), diesel generators, micro-hydro turbines, and battery storage. The solar PV type was chosen based on local irradiance data and typical efficiency ratings for rural applications, while the diesel generator was selected to provide reliable backup power during periods of low renewable generation. The micro-hydro turbine was specified according to the estimated head and flow rates at the selected sites, ensuring compatibility with run-of-river conditions. For energy storage, lead-acid batteries were considered due to their cost-effectiveness and suitability for off-grid systems, providing stability and storing excess energy for use during demand peaks or generation shortfalls. These components were parameterized in HOMER with technical and economic specifications reflective of locally available technologies and market conditions.

Hydropower potential assessment: It is considered one of the easiest, most reliable, and environmental friendly source of energy, Equation 10 was used to compute the power output of the hydro turbine.

$$P = \eta_{tr} \times \gamma_{wr} \times H_{net} \times Q_t \quad (10)$$

Where P is the power output [kW]; η_{tr} is turbine efficiency [%]; γ_{wr} is the specific gravity of water [9.81 kg m^{-3}]; H_{net} is the net head (m) and Q_t is the flow rate (m^3/s). The simulated stream flows of the selected three sites at their outlet corresponding to a 90% probability of exceedance (Q_{90}) were used in this study.

Solar power potential assessment: The solar energy resource assessment used bias-corrected ERA5 meteorological data (1991-2022) and local gauge records to fill gaps and derive site-level inputs (radiation, temperature, cloud cover) for the HOMER techno-economic runs. Using ERA5 solar radiation data and geographic coordinates of the Kulfo Catchment (approx. 6° N, 37° E), the average astronomical day length ranges from 11.8 h in December to 12.2 h in June. For standard solar resource modeling, Air Mass 1.5 (AM1.5) corresponds to a solar zenith angle of 48.19°, which yields an effective solar window of about 9.5–10.0 h per day under clear-sky conditions in this region. The Solar power potential assessment power output of PV cell was calculated by equation 11 is well described in [53];

$$P_{PV} = Y_{PV} f_{PV} \times \frac{G_T}{G_{T,STC}} \times \left[1 + \alpha_P (T_C - T_{C,STC})\right] \quad (11)$$

where $Y_{PV}$is the rated capacity of the PV array, which is the power output under standard test condition (kW), f_{pv} is PV rating factor (%), G_T is the incident solar radiation on the PV array in the current time step (kW/m^2), $G_{T,STC}$ is the incident radiation at standard test conditions (1 kW/m^2), α_p is the temperature coefficient of power, $T_C$is the PV cell temperature in the current time step (°C) and $T_{C,STC}$is the cell temperature under standard test conditions equal to 25°C.

Pre-simulation for sensitivity analysis before running HOMER software involves defining and preparing the key input parameters whose variability could significantly affect system performance or economic feasibility. This step includes identifying critical variables (e.g., fuel price, load demand, solar irradiance, wind speed, capital cost) and assigning realistic value ranges based on historical data, site-specific measurements, or literature. The aim is to ensure that the chosen variations reflect plausible real-world uncertainties so that the subsequent HOMER simulation can evaluate system robustness and identify the most influential factors.

The grid extension comparison evaluates different approaches to expanding the existing electrical grid by analyzing key parameters such as capacity, coverage area,

Table 6. Groups of criteria used

Economic criteria	Environmental Criteria	Social criteria Technical	Technical technological criteria	Others
Investment cost	Land use	Job creation	Resources availability	Safety
Net present cost Operation and maintenance cost	Visual impact Greenhouse gas (GHG)	Social benefits Social acceptability	Efficiency	Reliability Accessibility

reliability, and cost-effectiveness. It includes assessment of current grid infrastructure limits, potential new transmission lines, substation upgrades, and integration of renewable energy sources. Expansion plans focus on meeting growing demand, reducing losses, and enhancing grid stability while balancing investment costs and environmental impacts. The average useful grid extension distance is roughly up to 40 km for this study, beyond which off-grid solutions like micro hydropower are likely more practical and cost-effective for rural electrification.

2.13 Estimation of load demand of the selected areas

Load demand assessment

In a rural region where society has little knowledge about energy. Electronic devices and the assessment of load demand based on community concerns have been challenged. To assess the current load assessment we use Population size of the selected kebele and Status of energy were identified then to assess current and future load assessment. The data are collected demographic data of kebeles from Gamo statistics office and from Ethiopian electric utility Gamo distinct. The most practical and trustworthy method of determining the energy demand in the study areas is to compute the power demand requirements of energy consumption and population size for the current time and forecast the future period. The quantity of light bulbs and other significant, often used electrical devices in the research area was counted. Furthermore, it has calculated the amount of time and energy that electronic devices require on a daily basis. The hours that radio and television (TV) are most frequently utilized in Ethiopia are 7:00 am to 9:00 am, 11:00 am to 2:00 pm, and 6:00 pm to 11:00 pm, respectively. In this study area, a similar trend was implemented, to determine the energy requirement of each family, three light bulbs, one radio, one television, a mobile charger with a capacity of 150 liters, one baking plate, and energy for various cooking devices were used.

Population forecasting

The size of the population is a standard factor used to forecast the future electricity demand of rural communities. In order to create some expectations and ultimately determine the demand based on future population predictions, the load demand of the area has been determined. The chosen rural potential site's future population size has been predicted using the geometrical increase technique [54]. The statistical Gamo zone was used to collect the population data for each kebele. The forecasted population size was calculated below in Equation 12.

$$n = P_0(1 + r/100)^n \tag{12}$$

Where; P_0 is the present population size; P_n is the population at the n^{th} year; n is the number of years and r is the geometric growth rate (%). Because, in Ethiopian population growth particularly in rural areas the growth rate is 2.9 percent by [55]. The current total population and total number of households to be electrified by the proposed system was 42,883 and 10,555 respectively. From current total population and total number of households to be electrified are 8510 and 2128 respectively. The future estimated total population and total number of households to be electrified by the proposed system was 65,844 and 13,169 respectively to be estimated.

Forecasting Rural Energy Demand Supply Balance

Load forecasting is a technique used to estimate the load for a future period from the available past data. In addition, it is a crucial and essential in the operation and control of electric utilities. The hourly total load system is often the basic quantity load forecasting. It includes the accurate forecasting of the sizes and locations of the electric load for the various (often-hourly) planning limit intervals. Load forecasting play an important role in Power operation, control and energy planning [56].

The load demand in this study is categorized into three groups these are domestic, community and deferrable load respectively. Domestic load consists of lights, home electric appliances including TV, Tape, and mobile charger etc. The domestic load equation as shown below in equation 13.

$$\text{Domestic load} = \sum \begin{pmatrix} (\text{light point load in 1hr}) \\ + (\text{Tape recorder load in 1hr}) \\ + (\text{Mobile charge load in 1hr}) \end{pmatrix} \tag{13}$$

Community load also service load gives to service for the community such as schools, health centers, churches, and mosques. Hence, for each service, the load demand

for a given hour was calculated by equation 14.

$$\text{Community load} = \sum \left(\begin{array}{l} \text{(School External light)} \\ +\text{health center(Room light} \\ +\text{External light+Vascine Freeze)} \\ +\text{church and mosques(light point} \\ +\text{Mega point)} \end{array} \right) \quad (14)$$

The primary load in my study was calculated based on the low income of the community in the village. In addition, the sum of domestic and community load is given by equation 15.

$$\text{Primary load} = \text{Community load} + \text{Domestic load} \quad (15)$$

Deferrable load is used under special conditions and the exact time is not known. The primary and deferrable loads are input for the HOMER model. The real operating factor of PV should be considered by temperature effect, Irradiance variation, dust, and panel.

Economic analysis of hybrid energy and selection of feasible configuration

The economic study of decentralized energy systems has been crucial because it helps us compare the costs of different energy sources. HOMER uses discount rates to convert one-time costs into comparable annual costs and the annual interest rate has priced to increase uniformly. This is roughly equivalent to the nominal interest rate less than inflation rate. All costs in HOMER are real costs, which mean that they are express in terms of fixed dollars. Through taking into account all expenditures incurred throughout the system's life, life-cycle cost analysis achieves by [57].

$$\begin{aligned} \text{NPC}_{tot} &= \text{Cap}_{tot} + \text{CO\&M}_{tot} + \text{CRF}_{tot} \\ &\quad +\text{Total revenue of the project} \quad (16) \\ C_{ann.tot} &= (\text{CRF}) \times \text{NPC}_{tot} label17 \quad (17) \\ (\text{CRF}) &= i\frac{(1+i)^n}{(1+i)^{n_1}} \quad (18) \end{aligned}$$

Where: NPC_{tot} is total net present cost, Cap_{tot} is total capacity, $\text{CO\&M}_{tot}$ is operational and maintenances cost, CRF_{tot} is total capital recovery factor, $C_{ann.tot}$ is total annualized cost ($/year) and (CRF) is capital recovery factor.

The Levelized cost of energy (LCOE) is the average cost per kWh of useful electrical energy and it is often a convenient metric with which to compare the costs of different systems. HOMER uses the total NPC instead of as its primary economic cost. HOMER were calculate the Levelized cost of energy (LCOE)

$$\text{LCOE} = \frac{C_{ann.tot}}{\text{E}_{prim} + \text{E}_{def} + \text{E}_{grid,scale}} \quad (19)$$

Where; $C_{ann.tot}$ is the total annualized cost, E_{prim} the total amounts of primary load and E_{def} is deferrable load that the system serves per year and $\text{E}_{grid,scale}$ sale is the amount of energy sold to the grid per year

The system in the denominator of equation annually was expressed in equation (17). The average cost per kilowatt-hour of usable electrical energy generated by the system is consequently the Levelized cost of energy. NPC rather than Levelised cost of energy to rank the system configurations during its optimization process. This is due to the definition of the Levelized cost of energy being more debatable than the definition of the total NPC. The economic feasibility of hybrid systems, such as the micro-hydro and solar PV configurations assessed in the Kulfo Catchment, depends on optimizing technical performance and minimizing costs while ensuring reliable rural electrification. The market penetration of renewable energy technologies in the power production system is heavily influenced by cost, which is one of the most significant market drivers. Examining how adding external additional battery storage may affect the COE using the HOMER model [58].

The capital cost of the photovoltaic (PV) system comprises several key components, including PV modules, inverters, balance-of-system (BOS) components (such as mounting structures, cabling, combiner boxes, and protection devices), site civil works, transport, and installation/labour and commissioning. A contingency typically 5 %–10 % of total capital expenditure is often added to account for unforeseen expenses; this also includes preliminary or pre-operating costs like insurance, logistics, and financing. Local taxes, fees, and permitting costs are similarly included, often represented as a percentage of the total capital cost.

Based on the requirement to incorporate detailed cost inputs for the HOMER techno-economic simulation, the capital costs, replacement costs, and operation and maintenance (O&M) costs for each system component including micro-hydro turbines, solar PV panels, battery storage, and diesel generators must be defined using current market value. For instance, the capital cost of micro-hydro systems typically ranges from $2,000 to $5,000 per kW depending on site-specific conditions such as head and flow [30] while solar PV capital costs in sub-Saharan Africa are estimated at $800–$1,200 per kW [23]. Battery storage systems, particularly lead-acid types commonly used in off-grid hybrid systems, may incur capital costs of $200–$300 per kWh with O&M costs around $10 per kW/year [58]. Diesel generators have a lower initial capital cost of approximately $300-$500 per kW but higher O&M and fuel costs, often ranging from $0.02 to $0.05 per kWh [15]. These cost assumptions should be validated against local market surveys and recent literature to ensure accuracy and relevance to the Ethiopian context.

3. Results and Discussion

3.1 Bias Correction of ERA5 Satellite Data

It has been a priority to remove biases in satellite observation to get capable historical meteorological data. It has been essential for this aim to have a metrological gauge station with a complete parameter (class-I) and data length in the research area under study. The remaining weather stations are all class 3 or class 4, with the exception of the Arba Minch station in the watershed's

https://doi.org/10.57647/ijeee.2024.1501.08

upstream region.

When the gap was wide, less information on climatic parameters was taken, and vice versa. Important HOMER input data, such as wind speed, sunshine hour, cloud cover, and clearness index, are not captured at class 3 or class 4 stations. Accordingly, by applying the identical climate variables at the Arba Minch station, the biases at these stations were eliminated. This principle was used to conduct bias correction for all sites that were found to have bias-corrected climate variables along the Kulfo Catchments. This study used the power transform technique among different methods.

3.2 Spatio-temporal Distribution of Hydro- meteorological Data

Spatial distribution of rainfall in the catchment

Based on Ethiopia's climatic classification, the Kulfo Catchment has a tropical climate with hot, semi-arid temperatures. The annual rainfall ranges from 665mm to 1240 mm, with average minimum and maximum temperatures of 13.9 °C and 31.2 °C [59]. The region has seen bimodal rainfall, with April and October seeing the highest levels. Many variables, such as elevation, slope, and predominant wind directions, can affect the spatial variance of rainfall. This depends on the geographical and climatological characteristics of the study area. Therefore, the rainfall geographical distribution of bias-corrected ERA5 satellite data on the Kulfo Catchment is displayed in Figure 9 below.

The above Figure 9 showed that the studied area of the spatial distribution of rainfall depending on the location and selective feasible site. Rainfall distribution over the area was received ranging from 440mm to 1300mm per annum. This shows that the area over the year gains major rainfall receives. In addition, the area has bimodal rainfall practiced within the year two months has maximum rainfall obtained during April and October. Overall, the topography of mountainous regions differs from that of plain regions in terms of the spatial distribution of precipitation. Additionally, the average precipitation distribution offers crucial information for comprehending the hydrological process.

Figure 10 above shows that the mean monthly temperature in the watershed ranges from 23.9°C in the northern area and 26.29°C in the southern area of the watershed. The center section of the watershed has been hot climate, with average temperatures ranging from 24.52°C to 25.1°C. The spatial distributions of temperature on the studied area affected the point of temperature concerning feasibility site and location.

The above Figure 11 showed that the solar radiation in the watershed varying from 7.2w/m^2 to7.8w/m^2 .The location is suitable for solar power generation due to the hot temperatures and high sunshine hours. Generally, energy from sunlight was not spread evenly over earth. On the dayside, only the area directly beneath the sun is exposed to full solar radiation.

The above Figure 12 shows that the spatial distribution of ERA5satelitte bias corrected cloud cover (fraction). This study was used to identify the area having clearness of the sky. Cloud cover is also another essential input parameter of HOMER with a value ranging from 0.12-0.29 taken in this study.

Temporal distribution of rainfall in the catchment

Rainfall in the watershed has been bimodal mainly rain season is the Belg season, which is May, April and March (MAM). From those months April is the maximum rain receive. The second rainy season is Bega (OND). In this case, the season was the maximum rain received during October. The area has been about 80% of the rainfall during the Bega and Belg seasons. In general, Southern Nations, Nationalities, and Peoples (SNNPE) have bimodal rainfall distribution. The Thiessen polygon method was used to calculate the research area's areal rainfall. The Annual cycle of bias-corrected ERA5 satellite data of Mean monthly temperature and annual rainfall is shown below in Figure 13.

The above Figure 13 showed that the results of the mean monthly temperature and annual rainfall during Belg (MAM) the main rainy season over the studied area are peak at April. The second season is Bega such as September, October and November (SON) high amount of rainfall having the October month received. The maximum temperature of the studied area was recorded on the January to March and on June to August per month.

The above Figure 14 result showed that the maximum solar radiation over the studied area occurred during the bulk of January through June. From those months, the peak solar radiation occurred during February is 7.8 w/m2. While the minimum solar radiation occurred between May and September (3.8–4.2) w/m2. The maximum cloud cover over the studied area occurred from June to August. However, minimum cloud occurred except between June and August.

3.3 Modeling stream flow of Kulfo Catchment using HBV-IHMS

Sensitivity analysis

The sensitivity analysis has been carried out by changing the parameter values within the allowable range. All parameter values correspond to the time step of the day. Each parameter's value changed while the values of the other parameters remained constant. Among the response unit parameters are those included in response routine parameters such as Perc, Alfa, K4, and Khq in terms of NSE and RVE. The model simulations are susceptible to variations in the parameter's value. The NSE and RVE values in the Kulfo catchment remain constant over a wide range of values of Perc, Alfa, K4, and Cflux. These parameters are simulated hydrographs, which indicates that they do not control the pattern.

Furthermore, changes in the values of FC, Beta, LP, and Cflux all of which fall under the category of soil moisture routines also result in significant changes in RVE, indicating that the simulated flow was regulated

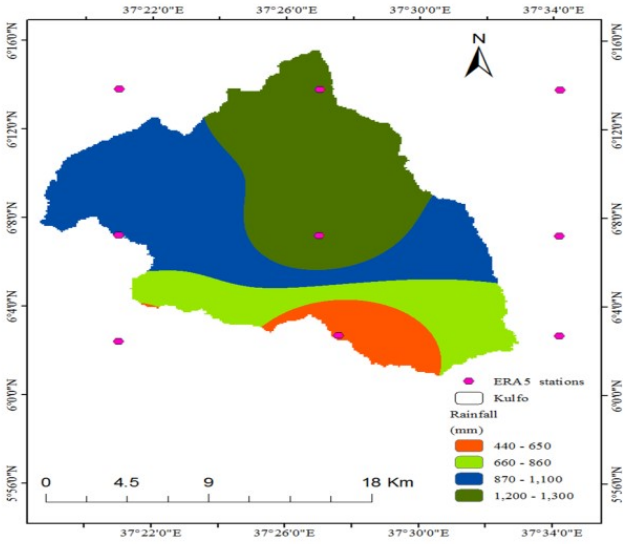

Figure 9. Spatial distribution rainfall (mm) of bias-corrected ERA5 satellite data

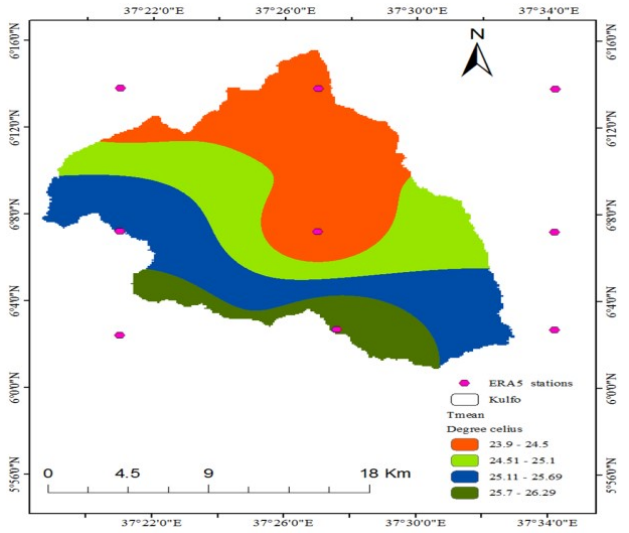

Figure 10. Spatial distribution rainfall (mm) of bias-corrected ERA5 satellite data

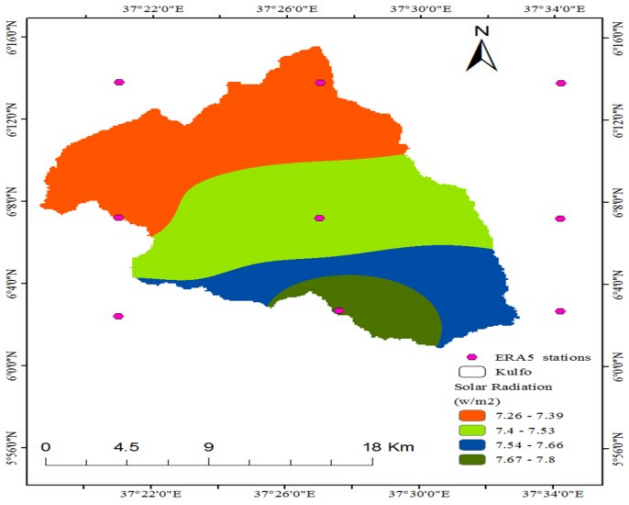

Figure 11. Spatial distribution of bias corrected ERA5 satellite Mean temperature (°C)

https://doi.org/10.57647/ijeee.2024.1501.08

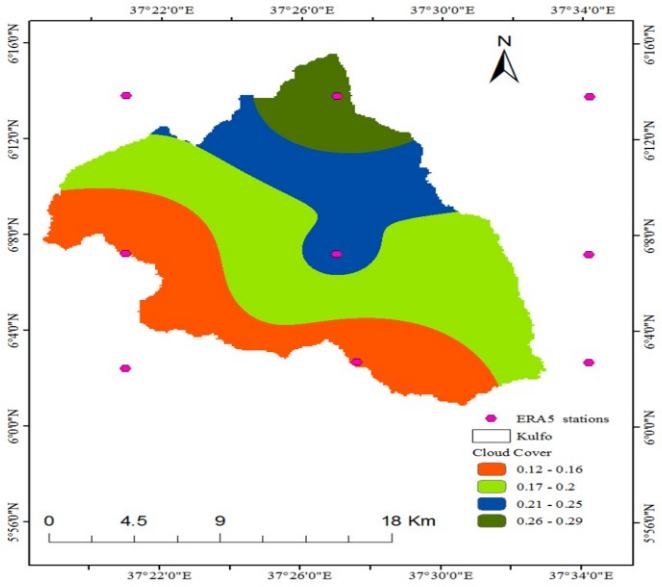

Figure 12. Spatial distribution of ERA5satelitte cloud cover (fraction)

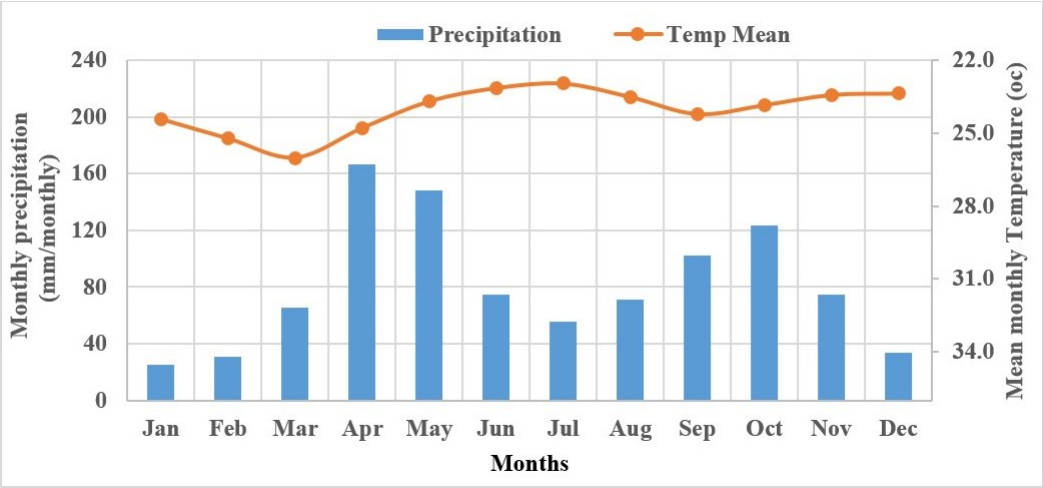

Figure 13. Annual cycle bias-corrected ERA5 satellite data of Mean monthly temperature (°C) and annual rainfall (mm)

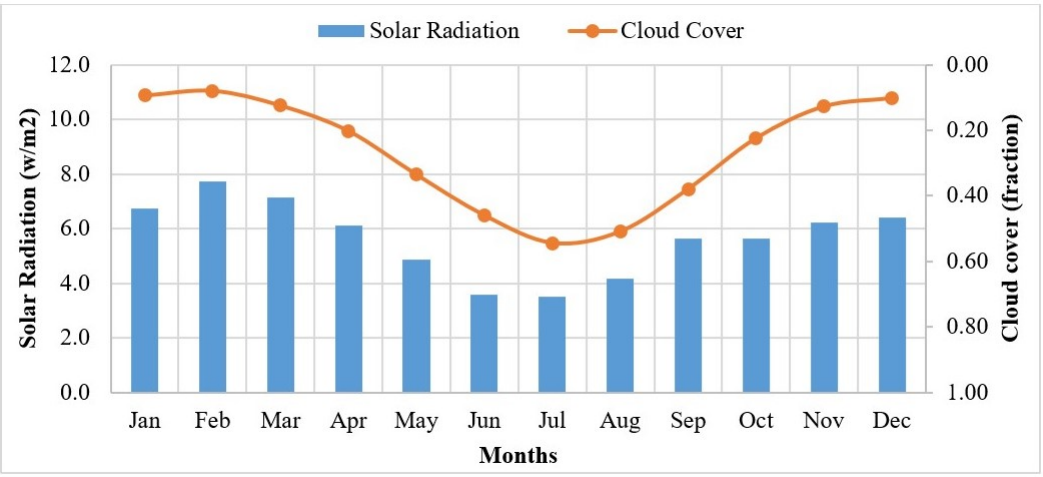

Figure 14. The distribution of solar radiation (W/m2) and cloud cover (fraction)

https://doi.org/10.57647/ijeee.2024.1501.08

in these three parameters. The field capacity (FC) characteristic influences runoff rate and is associated with maximal soil water storage; a higher FC often results in a higher base flow and a lower peak flow. The Khq and Alfa parameters are related to peak flow; the higher the values of these parameters, the higher the peaks and the more dynamic the hydrograph response. The parameters Perc, K4, and Cflux are associated with base flow and decline parameters.

Calibration and Validation

The model was manually calibrated by varying each parameter's value one at a time within the permitted range to produce the calibrated parameter values. After the sensitive parameters were identified using sensitivity analyses, automatic calibration methods were employed in the model's calibration using the observed monthly stream flow for a period (1993-2006 When calibrated parameters from this measuring station are used to predict river flows across the entire watershed, the actual flow is underestimated. This results from a lack of data in the watershed and is the cause of the unreliability of earlier estimation attempts. The simulated and actual hydrographs in the Kulfo catchments are displayed in Figure 15. The model does a good job of capturing the base flows of the hydrograph and appropriately depicting the recession limb.

After calibration, the model was validated using its final best-fit parameters. For the period (2007-2013), calibrated parameters were validated. Monthly validation steps and statistical evaluation of the model consistency were performed using observed flow data. The output of the model was then compared to actual stream flow measurements recorded at the Arba Minch gauging station in the Kulfo. In Table 7 result With a Nash-Sutcliffe simulation efficiency (NSE) of 0.69 and Relative volume error (RVE) of -1.07% as a consequence of validation, monthly flows that were measured and simulated had very good performance level of agreement. For both the calibration and validation periods, Figure 15 above demonstrates that the observed and simulated values coincide very well. That is, the graphs for observed data and the corresponding simulated values show similar patterns. For further study need of refinement and recalibration are necessary extend for the calibration/-validation period if additional observed streamflow data becomes available.

The values of the objective functions and the calibrated model parameters are shown in Table 8. All catchments had NSEs above 0.6 throughout the calibration period, demonstrating how well the model captured the observed hydrograph pattern. The model accurately replicated observed stream flow volumes, as indicated by the RVE values falling between -5% and +5%. During the Arba Minch validation period, the model's performance improved with regard to the objective function (NSE).

Simulation of streamflow at selected potential hydropower site and head assessment in Kulfo catchment

The portion of the Kulfo catchment in selected rural kebeles characterized lack of electricity namely in T'sayte, Wisamo, Gatse, and Mazo Doysa was classified as the main scarcity area. Micro Hydropower and solar hybrid system potential sites were chosen based on the information that was available, the sites' accessibility to the community, and their availability. However, stream flow data is not available evenly at all four of the sites that were chosen. Every location's stream flow was simulated using the HBV model. The selected potential sites with flow duration curve and kebeles are described in Figure 16 and Figure 17 below. Through actual examination of the head drops at the sites, the head available in the catchment was determined to be 30, 30, 28, and 35 meters for T'sayte, Wisamo, Gatse, and Mazo Doysa, respectively.

The HBV-IHMS model used to simulate the mean monthly stream flow of the selected sites using the same characteristics flow along the Kulfo catchment took meteorological data from 1991 to 2020. The model's input was used to calculate the Catchment's physical properties. The mean monthly simulated site flow from the IHMS model and the output entered into the energy model to determine the hydropower were used to create the flow of the sites that were identified.

3.4 Demand and Energy Situation in Selected Kebeles of Community

Summary of the energy status of the selected sites and future population

The total population size in 2022 was 42,883 and out of the total population energy used of the selected kebeles namely T'sayte, Wisamo, Gatse, and Mazo doysa were 1500, 2010, 2000, and 3000 respectively. Likewise, over the studied kebeles 8510 of the population obtained electricity while 34,373 would not use electricity this represents the majority of the community's lack of electricity. The estimated population size energy not used after the fifteenth year (2037) will be 52,777. Besides, the approximate number of households is 10,555. According to the combined results of the four selected kebeles seven out of 10 people in the community lack access to electricity. From collected demographic data calculated of the total population and the energy forecast were conducted considering electricity used parts of the community in the next 15 years.

The results in Table 9 revealed that the total population size of the selected kebeles namely T'sayte, Wisamo, Mayzo doysa, and Gatse kebeles were 7517, 11972, 10687and 12707 respectively and the Size percent of kebeles were 17.53, 27.92, 24.92 and 29.63. In addition, the total population of energy used in percent on the kebeles were 19.95, 16.79, 18.71and 23.61 respectively. However, energy not used in percent of kebeles was 80.0, 83.2, 81.3 and 76.4. Overall, out of the total population, 42,883 of the studied kebele about 8510

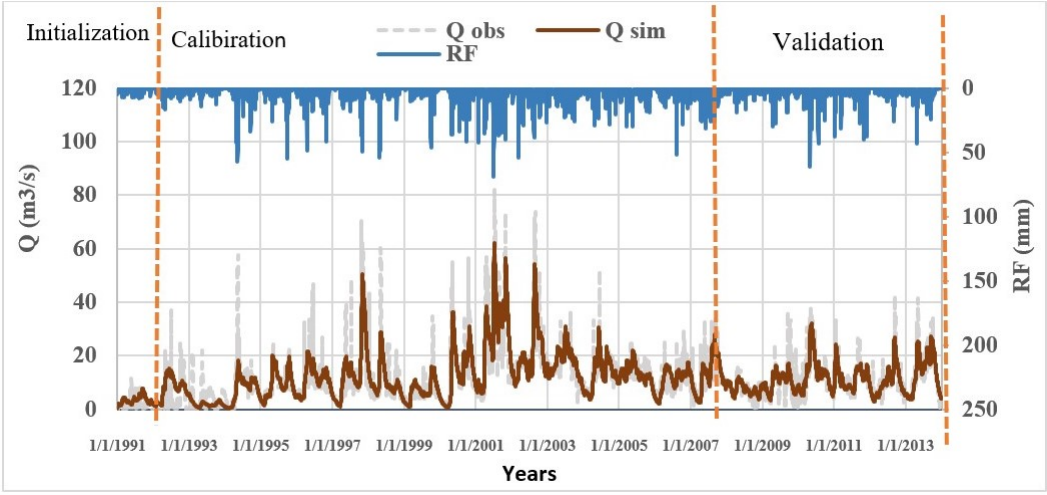

Figure 15. Observed and simulated monthly discharge graph for the IHMS calibration and validation results for the period (1993-2006) and (2007-2013) respectively

Table 7. Simulation results for the calibration and validation periods

No	Measure	Equations	Recommended value
1	NSE	$NSE = 1 - \frac{\sum_{i=1}^{n}(Q_{obs,i} - Q_{sim,i})^2}{\sum_{i=1}^{n}(Q_{obs,i} - Q_{obs,mean})^2}$	0.75-1 is Very good 0.65-0.74 is good
2	RVE	$RVE = \frac{\sum_{i=1}^{n}(Q_{sim,i} - Q_{obs,\ i})}{\sum_{i=1}^{n}(Q_{obs,i})} * 100\%$	-5% to 5% is well performed

Table 8. Calibrated value of model parameter and value of objectives

Model performance				Parameters								Remark
Calibration		Validation										
NSE	RVE	NSE	RVE	Alfa	Beta	Cflux	FC	K4	hq	LP	Per	Very good
0.69	4.56	0.63	-1.07	0.001	1	0.01	780	0. 037	1.39	0.45	0.01	

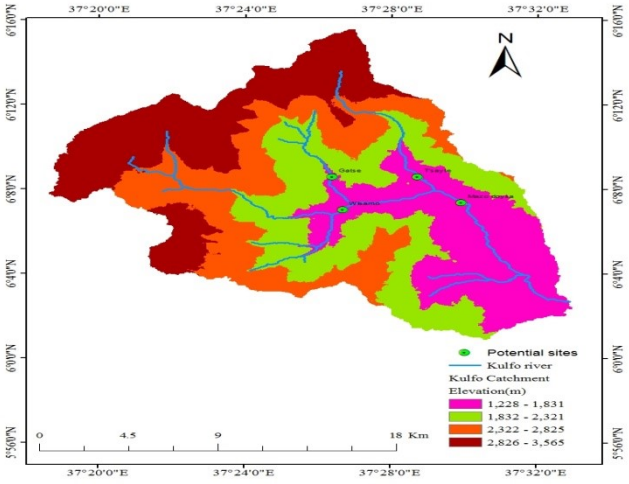

Figure 16. Main kebele of the selected potential site

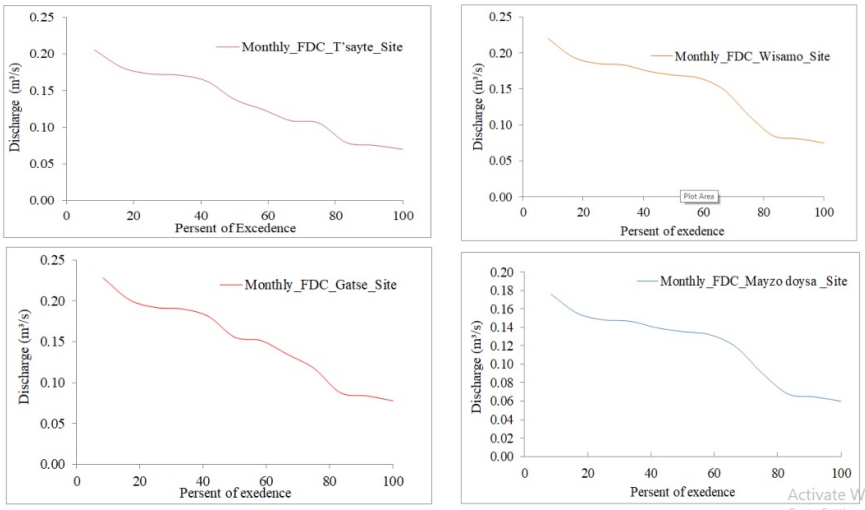

Figure 17. Flow Duration Curve (FDC) of T'sayte, Wisamo, Gatse, and Mazo Doysa sites

Table 9. Population size of the selected kebele and Status of energy

S.No	Name of Kebele	Population size in 2022			Population size in (%)	Energy used used in (%)	Energy Not used in (%)
		Male	Female	Total			
1	T'sayte	3683	3834	7517	17.53	19.95	80.0
2	Wisamo	5866	6106	11972	27.92	16.79	83.2
3	Mayzo doysa	5237	5450	10687	24.92	18.71	81.3
4	Gatse	6226	6481	12707	29.63	23.61	76.4
	Sum			**42,883**	**100**	**19.77**	**80.2**

population obtained electricity. However, 34,373 populations would not use electricity.

Besides, Wisamo kebele was the lowest kebele that used less electricity at 16.3% while Gatse 23.3% more used electricity as compared with selected other kebele. In general, from the total population size of the selected four rural kebeles, the average energy used in percentage is 19.77%, and the energy not used is 80.2%. The total population of the four kebeles was 42,883 and the estimated population after fifteen years was calculated by geometric growth shown in equation 12. The population forecast for 2037 showed the total population size over the studied kebele to be 65,844 and the approximate number of households has to be the estimated population divided by the number of households to be 13,169.

The results in Table 10 revealed that during the hours of (1:00-2:00), (2:00-3:00), (3:00-5:00), (4:00-5:00), and (5:00-6:00) at night, appliances such as lights, mobile chargers, tape recorders, televisions, and stoves were not used. Although a household needs electricity for lighting, running a radio or TV, and powering mobile devices, this loads a television (30 W), a phone charger (5 W), and compact fluorescent lights (11 W) for each family in the village. The typical daily operation time for TVs, radios, and light bulbs is two average daily TV/radio operating time is 2 h for light bulbs about four hours per day. As a result, it is not connected to the national grid.

Besides, in this studied area from (12:00-17:00) each hour of the time could not be used Refrigerator (23:00-1:00) and Injera Mitad regarded the community as having a low-income community. Deferrable load in watt-hour (Wh) used under special conditions when needed from the community from 7:00-10:00 for every hour. However, the power consumption of the community in watt-hour was used every hour. In addition, the community load indicated every hour in the years working the appliances namely Health center, Church, Mosques, and floor mail. On the Sunday from community load, the floor miles were not working except for churches and health centers. Further, the primary load was calculated shown in equation 14 the sum of energy in watt-hour of domestic and community. Finally, the total load as described in the above table the sum of the domestic and social load of the selected kebeles.

3.5 Diurnal Cycle of the Hybrid Power System Estimated Using HOMER

Figure 18 below reveals the daily difference in the hydropower output from the selected site. Based on the figure shown, for the first 90 days, the light blue color indicates that the hydropower output is low. At this time, the HOMER was simulating another alternative renewable resource. However, between 90 and 180 days the power would be increased. Accordingly, the red color indicates

Table 10. Hourly average power load of the Potential site

Time of power consumption (hr)	Domestic Energy (Wh)	Community (Wh)	Primary load (Wh)	Deferrable (Wh)	Total load (Wh)
01:00-02:00	0	4525.63	4525.63		4525.63
02:00-03:00	0	19540.68	19540.68		19540.68
03:00-04:00	0	19540.68	19540.68		19540.68
04:00-05:00	0	19540.68	19540.68		19540.68
05:00:06:00	0	4525.63	4525.63	148500	153025.63
06:00-07:00	569991.6	2308.99	572300.59	148500	720800.59
07:00-08:00	11716494	1873.58	11718367.58	148500	11866867.58
08:00-09:00	105554	1319.43	106873.43	148500	255373.43
09:00-10:00	0	16334.48	16334.48	148500	164834.48
10:00-11:00	1055540	16334.48	1071874.48	148500	1220374.48
11:00-12:00	10555400	16334.48	10571734.48		10571734.48
12:00-13:00	0	3430.51	3430.51		3430.51
13:00:14:00	0	3430.51	3430.51		3430.51
14:00-15:00	0	3430.51	3430.51		3430.51
15:00-16:00	0	3430.51	3430.51		3430.51
16:00-17:00	0	1319.43	1319.43	148500	149819.43
17:00-18:00	0	1319.43	1319.43	148500	149819.43
18:00-19:00	10660954	8858.62	10669812.62	148500	10818312.62
19:00:20:00	1731085.6	7974.60	1739060.20		1739060.20
20:00-21:00	1625531.6	9294.03	1634825.63		1634825.63
21:00-22:00	1625531.6	9294.03	1634825.63		1634825.63
22:00-23:00	569991.6	4881.87	574873.47		574873.47
23:00:00:00	0	4446.46	4446.46		4446.46
00:00-1:00	0	4525.63	4525.63		4525.63
Sum	40216074	187814.871	40403888.87	1336500	41740388.87

the maximum hydropower output produced. Moreover, the entire catchment's high rainfall was obtained during April and October. In this case, the batteries operated to store the surplus amount of energy for future use. As a result, the community received approximately 61.3% of its energy from hydropower output.

The daily Photovoltaic power output shown below the Figure 19 lowered during October and April and solar energy was not generated in those months. Besides, load coverage during the peak hours (18:00-24:00) and at night (1:00-7:00) was quite difficult. However, the maximum solar energy produced at 6:00-12:00 hours is shown the yellow color but, the dark color indicates solar power does not occur. During this time another alternative energy source that is hydropower, compensates power to deliver to the community before account shortage of power.

As seen in Figure 20 below, the hybrid system's resulting daily cycle of generator output demonstrated that the system's demand energy was compelled to use the generator's maximum capacity due to the decreased rainfall and solar radiation. These sources are significant for increasing hydro and solar power. Hence, both stand-alone hydropower and solar production were unable to meet the system's energy demand, forcing it to use its generators to the fullest extent possible. The generator used when renewable energy deficits occur needs backup energy and is expected to operate for the bulk of the time. In this study for HOMER simulations, the most commonly utilized generator type was the diesel generator.

The above Figure 21 shows that the battery was able to fully charge at this time due to the significant hydropower output. Hydropower production increased in absolute terms during periods of electricity scarcity from April to October 30 before beginning to fall in December. The battery was fully charged for the entire month thanks to the battery's ability to store a lot of energy during this time.

The battery is a crucial component of the hybrid system since it keeps the microgrid's operation stable while storing excess energy and supplying needed energy. HOMER using the kinetic battery model determines the quantity of energy that can be absorbed by or removed from the battery storage for each time step. The allowable range is determined by the maximum charge and discharge power. For the time step electricity going into and coming out of the battery storage.

The most practical configuration in this study to accommodate for daily energy fluctuations is hydropower coupled with solar power source and battery assistance. The power output from hydro is lower during the first 120 days of the year, from 1^{st} January to March 30 (Figure 21), and the load demand during this time can be fulfilled by combining solar energy and the condition of battery systems. The solar power output is quite low

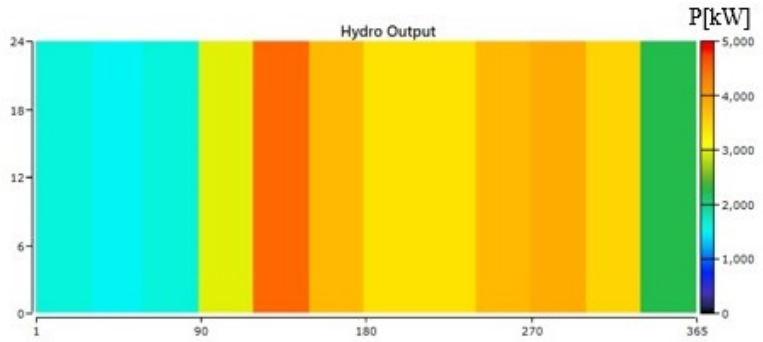

Figure 18. Diurnal cycle of hydropower output from the hybrid system

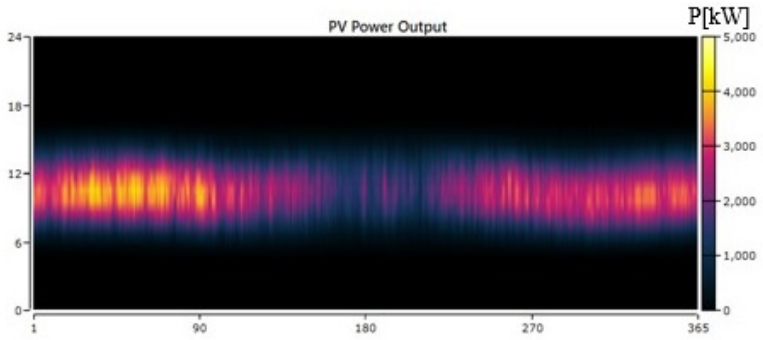

Figure 19. Diurnal cycle of solar power output from the hybrid system

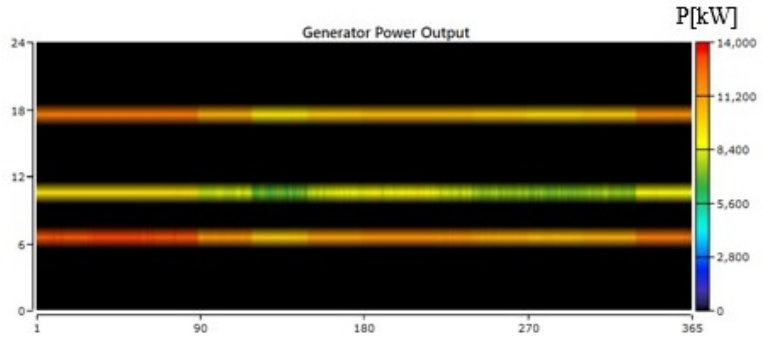

Figure 20. Diurnal cycle of generator output from the hybrid system

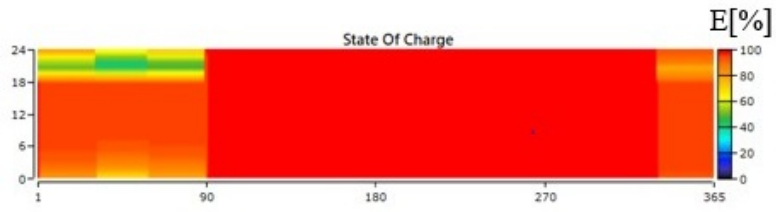

Figure 21. Diurnal cycle of battery output from the hybrid system

https://doi.org/10.57647/ijeee.2024.1501.08

from day 90 to day 270, especially between the hours of 0:00, 9:00, 15:00, and 24:00 Figure 20. Mostly, the load requirement of the site is only satisfied by hydropower at 61.3% as solar power covers 19.4%. This indicates that the maximum power obtained from hydropower than solar power. Hydropower is the best selected for this scheme depending on an economically viable solution for rural villages of those who have low income.

3.6 Economic Evaluation and Selection of Viable Hydro and Solar Power

The HOMER, model was repeated and run through the optimization process to find the lowest net present cost (NPC). The model has chosen over 3000 configurations based on their lowest Levelized cost of energy (LCOE) and total NPC. The main goal was to compute and contrast the system's LCOE under various conditions. These are the circumstances that are taken into consideration. In the first three scenarios, hybrid photovoltaic (PV), hydropower, and generators were considered sources of renewable energy. Generally, based on viable solutions, hydropower and generators were selected as photovoltaic (PV) resources were too expensive to implement in the studied area. The main support for the electricity load has been hydropower, making the renewable fraction about 55.6% in all configurations. The best configuration NPC is $81.2 million, which shows that investment costs are decreasing in all configuration hydro schemes mainly chosen for load coverage. Moreover, the Levelized cost of energy was 0.0962 less compared to other schemes. Besides, the annual power production of solar energy (PV), hydropower, and generators was 5,641,903, 27,566,199 and 11, 736, 523, kwhr/yr and the percent coverage of 12.6, 61.3, and 26.1 respectively. Based on LCOE, the economic study of the first three hybrid system options at the selected site was selected based on a technicality and economically viable solution as shown in Table 11.

In addition, the above table revealed that the top three configurations have Levelized costs of energy that are nearly the same, with LCOE's at 0.0962 dollars per kilowatt hour (kWh), which was determined to be slightly different contrasted to Ethiopian Electricity Corporation's (EEC) expense of 0.06 dollars per kWh. In each case, the initial investment of a PV system is significantly higher than that of hydropower. Similarly study was reported by [34].

The aforementioned Table 12 shows that in the first three months occurred energy deficit due to this shortage the generator is required to stabilize the demand supply system. In order to simulate how the system would function, the HOMER model determined the energy balance for each of the 8,760 hours in a year. It identifies the most efficient method of obtaining electricity from each resource after calculating and comparing the system's hourly electrical and thermal demands. Additionally, HOMER used to make decisions about the generator operation every hour, including whether to charge or discharge the batteries. In general, HOMER runs these power-balancing calculations for each system configuration and assesses its viability. Either the diesel generator or the storage battery can supply the load when it is low.

During simulation, HOMER performs the power balance calculation for each system configuration and evaluates whether it is viable. During peak demand, the diesel generator and storage battery run in parallel mode. This simultaneous functioning allows the diesel generator's capital cost to be reduced. Further, the demand of the community for domestic load, public, and deferrable load based on the use of the appliance selected was calculated and described in detail in chapter three.

4. Conclusion

This study aims to evaluate the feasibility of supplying electricity to specific rural kebeles using a hybrid off-grid micro-hydro and solar power system. The feasibility and cost-effective configuration of the hybrid systems required primary data from a field survey and secondary data from the Ministry of Water and Energy (MoWE), the Ethiopian Meteorological Institute (EMI), and ERA5 reanalysis climate data, which were collected and used to evaluate the potential of the selected sites. Energy consumption was calculated based on the demand of the low-income community. The hourly demand of the community was calculated by considering various appliances for domestic and residential loads, such as lights, cooking stoves, mobile and radio chargers, flour mills, and institutions. These data are used to optimize the HOMER model of each system and run the simulation. The outcomes of the simulations covered in the report demonstrate that each power source's output is more than sufficient to meet the load and can even supply more.

The development of reliable and effective renewable energy sources was put into practice, improving the community's rural villages' social and economic well-being. This is because of the application of new developments in modeling and satellite technologies. The potential of ERA-5 satellite data and the HOMER model to assess the techno-economic feasibility of solar and hydro systems in off-grid locations within the Kulfo watershed was the main emphasis of this thesis. The HBV-IHMS hydrological modeling program was utilized to determine the flow ungauged site, and the ERA5 satellite data was effectively utilized to close the gaps in the hydro-meteorological data. In general, hybrid systems have a somewhat higher LCOE than the national tariff; given the changes in the poor's way of life in rural areas, the acceleration of deforestation, and the development of renewable energy, it may be a viable alternative for electrifying those areas. The Levelized cost of energy (LCOE) and capital cost of the micro hydro system are less than those of the hybrid system. Because of this site's hydropower supplies, the writer believes that installing a standalone micro hydro system is both economically viable and pollution-free.

https://doi.org/10.57647/ijeee.2024.1501.08

Table 11. Hybrid system developed scenario

Configurations	Components	Annual power production (kwhr/yr)	Coverage (%)	NPC ($M)	LCOE ($M)	O and M ($M)
1	PV Generator Hydro	5,641,903 11,736,523 27,566,199	12.60 26.10 61.30	81.12	0.0962	1.58
2	PV Generator Hydro	9,389,721 11,435,529 27,566,199	19.40 23.60 57.00	81.21	0.0963	1.58
3	Generator Hydro	12,855,270 27,566,199	31.8 68.2	81.29	0.0964	1.61
4	PV Generator Hydro	12,549,467 11,535,275 27,566,199	24.30 22.30 53.40	81.37	0.0965	1.58
5	PV Generator Hydro	7,782,461 11,572,246 27,566,199	16.60 24.70 58.80	81.49	0.0966	1.59
6	PV Generator Hydro	17,470,415 11,256,520 27,566,199	31 20 49	81.52	0.0967	1.58

Table 12. Energy balance calculation of selected site

Months	Hydropower output (kw)	PV output (kw)	Generator output (kw)	Total Renewable output power (kw)	Demand (kw)	Energy Balance
Jan	1774.8	771.2	1499.1	2545.94	2887.2	-341.3
Feb	1571.8	881.8	1523.6	2453.63	2887.2	-433.6
Mar	1695.7	817.1	1505.1	2512.84	2887.2	-374.4
Apr	3126.7	699.4	1327.2	3826.13	2887.2	938.9
May	4621.1	555.2	1161.0	5176.33	2887.2	2289.1
Jun	3850.7	408.1	1293.3	4258.77	2887.2	1371.6
Jul	3470.5	402.9	1345.7	3873.41	2890.2	983.2
Aug	3552.2	477.6	1315.7	4029.81	2884.3	1145.6
Sep	3886.8	646.1	1242.2	4532.97	2887.2	1645.8
Oct	4077.4	645.1	1209.8	4722.54	2887.2	1835.3
Nov	3664.5	711.9	1248.3	4376.39	2887.2	1489.2
Dec	2379.7	731.5	1416.2	3111.22	2887.2	224.0

https://doi.org/10.57647/ijeee.2024.1501.08

Authors contributions
All the authors have participated sufficiently in the intellectual content, conception and design of this work or the analysis and interpretation of the data (when applicable), as well as the writing of the manuscript.
Availability of data and materials
The data that support the findings of this study are available from the corresponding author, upon reasonable request.
Conflict of interests
The author declare that they have no known competing financial interests or personal relationships that could have appeared to influence the work reported in this paper.

References

1. Ibrahim I, Hamam Y, Alayli Y, Jamiru T, Sadiku E, Kupolati W, Ndambuki J, and Eze A. A review on Africa energy supply through renewable energy production: Nigeria, Cameroon, Ghana and South Africa as a case study. Energy Strategy Reviews 2021; 38:100740. DOI: 10.1016/j.esr.2021.100740
2. Bishoge O, Kombe G, and Mvile B. Renewable energy for sustainable development in sub-Saharan African countries: Challenges and way forward. Journal of Renewable and Sustainable Energy 2020; 12. DOI: 10.1063/5.0009297
3. Agoundedemba M, Kim C, and Kim H. Energy Status in Africa: Challenges, Progress and Sustainable Pathways. Energies 2023; 16. DOI: 10.3390/en16237708
4. Dagnachew A, Choi S, and Falchetta G. Energy planning in Sub-Saharan African countries needs to explicitly consider productive uses of electricity. Scientific Reports 2023; 13:1–14. DOI: 10.1038/s41598-023-40021-y
5. Blimpo M and Cosgrove-Davies M. Electricity Access in Sub-Saharan Africa: Uptake, Reliability, and Complementary Factors for Economic Impact. Africa Development Forum Series. 2019. DOI: 10.1596/978-1-4648-1361-0
6. Yalew A. The Ethiopian energy sector and its implications for the SDGs and modeling. Renewable and Sustainable Energy Transition 2022; 2:100018. DOI: 10.1016/j.rset.2022.100018
7. Yvergneaux J. Comparative Study on Rural Electrification Policies in Emerging Economies. Tech. rep. International Energy Agency, 2010
8. Abrham A. The Amhara Region's Rural Electrification Projects: Effectiveness, Challenges, and Rural Transformation Implications. Ethiopian Journal of Business and Economics (EJBE) 2021; 11:1–21. DOI: 10.4314/ejbe/v11i1.1
9. Giesen N van de, Hut R, and Selker J. The Trans-African Hydro-Meteorological Observatory (TAHMO). WIREs Water 2014; 1:341–8. DOI: 10.1002/wat2.1034
10. Rogers D, Tsirkunov V, Kootval H, Soares A, Kull D, Bogdanova AM, and Suwa M. How to Improve Hydromet Services in Developing Countries? Tech. rep. Global Facility for Disaster Reduction and Recovery, 2019
11. Getie EM. Poverty of Energy and Its Impact on Living Standards in Ethiopia. Journal of Electrical and Computer Engineering 2020; 2020. DOI: 10.1155/2020/7502583
12. Tiruye GA, Besha AT, Mekonnen YS, Benti NE, Gebreslase GA, and Tufa RA. Opportunities and challenges of renewable energy production in Ethiopia. Sustainability (Switzerland) 2021; 13:1–25. DOI: 10.3390/su131810381
13. Ariaei AR, Fakhr MH, and Ahmadi R. Comparative Analysis of Hybrid and Single-Source Power Systems for Sustainable Electricity Generation for Remote Areas: A Case Study in Zahedan. International Journal of Photoenergy 2024. DOI: 10.1155/2024/1929512
14. Hassan Q, Algburi S, Sameen AZ, Salman HM, and Jaszczur M. A review of hybrid renewable energy systems: Solar and wind-powered solutions: Challenges, opportunities, and policy implications. Results in Engineering 2023; 20:101621. DOI: 10.1016/j.rineng.2023.101621
15. Al Abri A, Al Kaaf A, Allouyahi M, Al Wahaibi A, Ahshan R, Al Abri RS, and Al Abri A. Techno-Economic and Environmental Analysis of Renewable Mix Hybrid Energy System for Sustainable Electrification of Al-Dhafrat Rural Area in Oman. Energies 2023; 16. DOI: 10.3390/en16010288
16. Bahramara S, Moghaddam MP, and Haghifam MR. Optimal planning of hybrid renewable energy systems using HOMER: A review. Renewable and Sustainable Energy Reviews 2016; 62:609–20. DOI: 10.1016/j.rser.2016.05.039
17. Islam MMM, Kowsar A, Haque AKMM, Hossain MK, Ali MH, Rubel MHK, and Rahman MF. Techno-economic Analysis of Hybrid Renewable Energy System for Healthcare Centre in Northwest Bangladesh. Process Integration and Optimization for Sustainability 2023; 7:315–28. DOI: 10.1007/s41660-022-00294-8

18. Ajiboye OK, Ochiegbu CV, Ofosu EA, and Gyamfi S. A review of hybrid renewable energies optimisation: design, methodologies, and criteria. International Journal of Sustainable Energy 2023; 42:648–84. DOI: 10.1080/14786451.2023.2227294
19. Bell B, Hersbach H, Simmons A, Berrisford P, Dahlgren P, Horányi A, Muñoz-Sabater J, Nicolas J, Radu R, Schepers D, Soci C, Villaume S, Bidlot JR, Haimberger L, Woollen J, Buontempo C, and Thépaut JN. The ERA5 global reanalysis: Preliminary extension to 1950. Quarterly Journal of the Royal Meteorological Society 2021; 147:4186–227. DOI: 10.1002/qj.4174
20. Towner J, Cloke HL, Zsoter E, Flamig Z, Hoch JM, Bazo J, De Perez EC, and Stephens EM. Assessing the performance of global hydrological models for capturing peak river flows in the Amazon basin. Hydrology and Earth System Sciences 2019; 23:3057–80. DOI: 10.5194/hess-23-3057-2019
21. Vanella D, Longo-Minnolo G, Belfiore O, Ramírez-Cuesta J, Pappalardo S, Consoli S, D'Urso G, Chirico G, Coppola A, Comegna A, Toscano A, Quarta R, Provenzano G, Ippolito M, Castagna A, and Gandolfi C. Comparing the use of ERA5 reanalysis dataset and ground-based agrometeorological data under different climates and topography in Italy. Journal of Hydrology: Regional Studies 2022; 42:101182. DOI: 10.1016/j.ejrh.2022.101182
22. Urban A, Napoli CD, Cloke H, Kyselý J, Pappenberger F, Sera F, Schneider R, Vicedo-Cabrera A, Acquaotta F, Ragettli M, Íñiguez C, Tobias A, Indermitte E, Orru H, Jaakkola J, Ryti N, Pascal M, Huber V, Schneider A, Donato F de', Michelozzi P, and Gasparrini A. Evaluation of the ERA5 reanalysis-based Universal Thermal Climate Index on mortality data in Europe. Environmental Research 2021; 198. DOI: 10.1016/j.envres.2021.111227
23. Hailu A and Kumsa D. Ethiopia renewable energy potentials and current state. AIMS Energy 2020; 9:1–14. DOI: 10.3934/ENERGY.2021001
24. Dayaratna K, Furchtgott-Roth D, Pollard M, and Stern R. Powering Human Advancement: Why the World Needs Affordable and Reliable Energy. 2023
25. Ouedraogo N. Energy consumption and economic growth: Evidence from the economic community of West African States (ECOWAS). Energy Economics 2013; 36:637–47. DOI: 10.1016/j.eneco.2012.11.011
26. Asghar Z. ENERGY–GDP RELATIONSHIP: A CAUSAL ANALYSIS FOR THE FIVE COUNTRIES OF SOUTH ASIA. Applied Econometrics and International Development 2008; 8:14
27. Komarova A, Filimonova I, and Kartashevich A. Energy consumption of the countries in the context of economic development and energy transition. Energy Reports 2022; 8:683–90. DOI: 10.1016/j.egyr.2022.07.072
28. Jaiswal K, Chowdhury C, Yadav D, Verma R, Dutta S, Jaiswal K, SangmeshB, and Karuppasamy K. Renewable and sustainable clean energy development and impact on social, economic, and environmental health. Energy Nexus 2022; 7:100118. DOI: 10.1016/j.nexus.2022.100118
29. Gebreslassie M, Cuvilas C, Zalengera C, To L, Baptista I, Robin E, Bekele G, Howe L, Shenga C, Macucule D, Kirshner J, Mulugetta Y, Power M, Robinson S, Jones D, and Broto VC. Delivering an off-grid transition to sustainable energy in Ethiopia and Mozambique. Energy, Sustainability and Society 2022; 12:1–18. DOI: 10.1186/s13705-022-00348-2
30. Kougias I, Aggidis G, Avellan F, Deniz S, Lundin U, Moro A, Muntean S, Novara D, Pérez-Díaz J, Quaranta E, Schild P, and Theodossiou N. Analysis of emerging technologies in the hydropower sector. Renewable and Sustainable Energy Reviews 2019; 113:109257. DOI: 10.1016/j.rser.2019.109257
31. Bogdanov D, Ram M, Aghahosseini A, Gulagi A, Oyewo A, Child M, Caldera U, Sadovskaia K, Farfan J, Barbosa LDSNS, Fasihi M, Khalili S, Traber T, and Breyer C. Low-cost renewable electricity as the key driver of the global energy transition towards sustainability. Energy 2021; 227:120467. DOI: 10.1016/j.energy.2021.120467
32. Gielen D, Boshell F, Saygin D, Bazilian M, Wagner N, and Gorini R. The role of renewable energy in the global energy transformation. Energy Strategy Reviews 2019; 24:38–50. DOI: 10.1016/j.esr.2019.01.006
33. Deshmukh M, Sameeroddin M, Abdul D, and Sattar MA. Renewable energy in the 21st century: A review. Materials Today: Proceedings 2023; 80:1756–9. DOI: 10.1016/j.matpr.2021.05.501
34. Samatar A, Mekhilef S, Mokhlis H, Kermadi M, Diblawe A, Stojcevski A, and Seyedmahmoudian M. The utilization and potential of solar energy in Somalia: Current state and prospects. Energy Strategy Reviews 2023; 48:101108. DOI: 10.1016/j.esr.2023.101108
35. Rodrigues H, Capistrano G, Mello F, Zufelato N, Silveira-Lacerda E, and Bakuzis A. Precise determination of the heat delivery during in vivo magnetic nanoparticle hyperthermia with infrared thermography. Physics in Medicine and Biology 2017; 62:4062–82. DOI: 10.1088/1361-6560/aa6793

36. Geremew K, Gedefaw M, Dagnew Z, and Jara D. Current level and correlates of traditional cooking energy sources utilization in urban settings in the context of climate change and health, Northwest Ethiopia: A case of Debre Markos town. BioMed Research International 2014. DOI: 10.1155/2014/572473

37. Shan S, Genç S, Kamran H, and Dinca G. Role of green technology innovation and renewable energy in carbon neutrality: A sustainable investigation from Turkey. Journal of Environmental Management 2021; 294:113004. DOI: 10.1016/j.jenvman.2021.113004

38. Yirgu T, Yihunie Y, Assele A, and Wogayehu T. Land Use/Land Cover Dynamics and its Environmental Impacts in Kulfo Watershed, Gamo Highlands, South Western Ethiopia. Journal of Geography, Environment and Earth Science International 2020; 24:1–11. DOI: 10.9734/jgeesi/2020/v24i230197

39. Kouadio C, Kouassi K, Diedhiou A, Obahoundje S, Amoussou E, Kamagate B, Paturel J, Coulibaly T, Coulibaly H, Didi R, and Savane I. Assessing the Hydropower Potential Using Hydrological Models and Geospatial Tools in the White Bandama Watershed (Côte d'Ivoire, West Africa). Frontiers in Water 2022; 4:1–14. DOI: 10.3389/frwa.2022.844934

40. Pham L, Eldosouky A, Oksum E, and Saada S. A new high resolution filter for source edge detection of potential field data. Geocarto International 2022; 37:3051–68. DOI: 10.1080/10106049.2020.1849414

41. Nzeuga A, Ghomsi F, Pham L, Eldosouky A, Aretouyap Z, Kana J, Yasmine Z, Fokem A, Nouayou R, Abdelrahman K, Fnais M, and Andráš P. Contribution of advanced edge-detection methods of potential field data in the tectono-structural study of the southwestern part of Cameroon. Frontiers in Earth Science 2022; 10:1–15. DOI: 10.3389/feart.2022.970614

42. Liu Z, Yu X, Jia L, Wang Y, Song Y, and Meng H. The influence of distance weight on the inverse distance weighted method for ore-grade estimation. Scientific Reports 2021; 11:1–8. DOI: 10.1038/s41598-021-82227-y

43. Maulud D and Abdulazeez A. A Review on Linear Regression Comprehensive in Machine Learning. Journal of Applied Science and Technology Trends 2020; 1:140–7. DOI: 10.38094/jastt1457

44. Santos V dos, Calijuri M, and Assis L de. Land cover changes implications in energy flow and water cycle in São Francisco Basin, Brazil, over the past 7 decades. Environmental Earth Sciences 2022; 81. DOI: 10.1007/s12665-022-10210-5

45. Durai V and Bhardwaj R. Forecasting quantitative rainfall over India using multi-model ensemble technique. Meteorology and Atmospheric Physics 2014; 126:31–48. DOI: 10.1007/s00703-014-0334-4

46. Singh H, Dube A, Kumar S, and Ashrit R. Bias correction of maximum temperature forecasts over India during March–May 2017. Journal of Earth System Science 2020; 129. DOI: 10.1007/s12040-019-1291-6

47. Chen J, Arsenault R, Brissette F, and Zhang S. Climate Change Impact Studies: Should We Bias Correct Climate Model Outputs or Post-Process Impact Model Outputs? Water Resources Research 2021; 57:1–22. DOI: 10.1029/2020WR028638

48. Zong B, Song Q, Min M, Cheng W, Lumezanu C, Cho D, and Chen H. Deep autoencoding Gaussian mixture model for unsupervised anomaly detection. *6th International Conference on Learning Representations, ICLR 2018 - Conference Track Proceedings*. 2018 :1–19

49. Dube A, Singh H, and Ashrit R. Heat Waves in India during MAM 2019: Verification of ensemble based probabilistic forecasts and impact of bias correction. Atmospheric Research 2021; 251:105421. DOI: 10.1016/j.atmosres.2020.105421

50. Leys C, Klein O, Dominicy Y, and Ley C. Detecting multivariate outliers: Use a robust variant of the Mahalanobis distance. Journal of Experimental Social Psychology 2018; 74:150–6. DOI: 10.1016/j.jesp.2017.09.011

51. Zhao L, Xia J, Xu CY, Wang Z, Sobkowiak L, and Long C. Evapotranspiration estimation methods in hydrological models. Journal of Geographical Sciences 2013; 23:359–69. DOI: 10.1007/s11442-013-1015-9

52. Whitman J, Hiatt J, Mowery C, Shy B, Yu R, Yamamoto T, Rathore U, Goldgof G, Whitty C, Woo J, Gallman A, Miller T, Levine A, Nguyen D, Bapat S, Balcerek J, Bylsma S, Lyons A, Li S, Wong AY, Gillis-Buck E, Steinhart Z, Lee Y, Apathy R, Lipke M, Smith J, Zheng T, Boothby I, Isaza E, Chan J, Acenas D, Lee J, Macrae T, Kyaw T, Wu D, Ng D, Gu W, York V, Eskandarian H, Callaway P, Warrier L, Moreno M, Levan J, Torres L, Farrington L, Loudermilk R, Koshal K, Zorn K, Garcia-Beltran W, Yang D, Astudillo M, Bernstein B, Gelfand J, Ryan E, Charles R, Iafrate A, Lennerz J, Miller S, Chiu C, Stramer S, Wilson M, Manglik A, Ye C, Krogan N, Anderson M, Cyster J, Ernst J, Wu A, Lynch K, Bern C, Hsu P, and Marson A. Evaluation of SARS-CoV-2 serology assays reveals a range of test performance. Nature Biotechnology 2020; 38:1174–83. DOI: 10.1038/s41587-020-0659-0

53. Ayana M, Mada Z, Hatiye S, and Mohammed A. A compendious approach for renewable energy assessment based on satellite and ground truth data: Bilate catchment, Rift Valley Basin, Ethiopia. International Journal of Energy and Environmental Engineering 2022. DOI: 10.1007/s40095-022-00484-7

54. Leta S and Mesele F. Spatial analysis of cattle and shoat population in Ethiopia: Growth trend, distribution and market access. Ethiopia Strategy Support Program II (ESSP II), SpringerPlus 2014; 3:1–10

55. Rodrigues P, Dorresteijn I, Guilherme J, Hanspach J, Beenhouwer MD, Hylander K, Bekele B, Senbeta F, Fischer J, and Nimmo D. Predicting the impacts of human population growth on forest mammals in the highlands of southwestern Ethiopia. Biological Conservation 2021; 256. DOI: 10.1016/j.biocon.2021.109046

56. Khan A, Mahmood A, Safdar A, Khan Z, and Khan N. Load forecasting, dynamic pricing and DSM in smart grid: A review. Renewable and Sustainable Energy Reviews 2016; 54:1311–22. DOI: 10.1016/j.rser.2015.10.117

57. Shahgholian S, Taheri M, and Jahangiri M. Investigating the Cost-Effectiveness of Solar Electricity Compared to Grid Electricity in the Capitals of Middle Eastern Countries: A Residential Scale Case Study Sepehr. International Journal of Photoenergy 2023; 19. DOI: 10.1155/2023/8028307

58. Sambhi S, Sharma H, Bhadoria V, Kumar P, Chaurasia R, Chaurasia G, Fotis G, Vita V, Ekonomou L, and Pavlatos C. Economic Feasibility of a Renewable Integrated Hybrid Power Generation System for a Rural Village of Ladakh. Energies 2022; 15:9126. DOI: 10.3390/en15239126

59. Ayka A. Hydrological Models Comparison for Estimation of Floods in the Abaya-Chamo Sub-Basin. Tech. rep. 2008 :1–110